Development of a Progressive Failure Model for Notched Woven Composite Laminates

Daniel Christopher Munden

Thesis submitted to the faculty of the Virginia Polytechnic Institute and State University in partial fulfillment of the requirements for the degree of

Master of Science

In

Mechanical Engineering

Robert L. West

Gary D. Seidel

Reza Mirzaeifar

August 7th, 2018

Blacksburg, VA

Keywords: Woven Fabric Composite, Progressive Failure, Failure Criteria, Damage Model

Development of a Progressive Failure Model for Notched Woven Composite Laminates

Daniel Munden

ABSTRACT

As part of the Composite Technology for Exploration (CTE) project at NASA, woven fabric composites are being investigated for their use in Space Launch System (SLS) hardware. Composites are more difficult to analyze than isotropic materials and require more complex methods for predicting failure. NASA is seeking a method for predicting the damage initiation and propagation of woven fabric composites in order to utilize these materials effectively in SLS hardware. This work focuses on notched woven fabric composites under tensile loading. An analytical model consisting of a macro-level failure criterion and damage propagation was developed and implemented in explicit finite element analysis to simulate woven composite materials. Several failure criteria and propagation models were investigated and compared. A response surface was used to better understand the effects of damage parameters on the failure load of a specimen. The model chosen to have best represented the physical specimen used the Tsai-Wu failure criterion. Additional physical tests are needed to further validate the model.

Development of a Progressive Failure Model for Notched Woven Composite Laminates

Daniel Munden

GENERAL AUDIENCE ABSTRACT

A composite material consists of two or more different materials that are joined together to form a new material with improved properties. Woven fabric composites weave strips of fibers and a bonding material into a pattern to increase the material's ability to withstand loads in various directions. NASA is seeking a method to predict the conditions under which woven fabric composites will break. A greater understanding of the capabilities of woven fabric composites will help NASA improve the structures involved in space exploration. This work attempts to build an analytical model that can predict the loads under which a woven fabric composite will break in tension. Several different analytical theories were used to model a woven fabric composite and the results were compared with lab tests. One of the theories, the Tsai-Wu failure criterion, was selected as the best representation of the physical specimen. Further additional physical tests are necessary to further validate the analytical model.

CONTENTS

LIST OF TABLES

LIST OF FIGURES

LIST OF EQUATIONS

1 INTRODUCTION

Composite materials are the result of joining two or more constituent materials of different physical or chemical properties for developing a new material with improved properties. Advanced composites consisting of high strength, high stiffness fibers feature predominantly in the aerospace and automotive industries where performance is key. The ability to tailor composites allows for structures that match the strength of metals and significantly reduce weight. Composites in aerospace range from complete airplanes to wing assemblies, helicopter rotor blades, seats, and instrument enclosures [1]. Composites that utilize continuous fibers can be classified as unidirectional or woven. Unidirectional composite laminates consist of multiple plies or layers, which incorporate fibers running in a single direction. The plies in woven composite laminates consist of warp and weft strands of fibers, which can be intertwined, in a variety of patterns to lock the fibers together. Woven fabrics compromise the directional strength afforded by unidirectional composites due to the crimping of the strands but excel under multidirectional loading conditions and impact [2].

Composites are often used to reduce a structure's weight through eliminating unnecessary material and strengthening critical sections. The advantage gained using composites is diminished if analysts are overly conservative due to uncertainty in the material's behavior. Currently, the most reliable way to assess a composite's performance is by conducting physical tests and characterizing a laminate with a specific set of directional plies, also called the layup. This method is widely used in the aerospace industry and is a costly solution. While many analytical techniques have been developed to predict the stresses and strains of composites under different loading conditions, predicting nonlinear behavior and failure of composites is still an area of active research. A majority of the research is focused on unidirectional composites but the increasing use of woven composites has created a need for improved analytical techniques.

NASA is working to take advantage of the many opportunities composites afford by building on the existing knowledge and incorporating composites into more projects. The goal of their Composite Technology Exploration (CTE) project is to advance composite technologies that provide lightweight structures for future Mars missions [3]. As part of this initiative, NASA seeks to improve composite bonded joint technology. One of the limiting design aspects of

bonded joints is predicting the failure of woven fabric composites. Improving woven composite failure analysis has been identified as an important step in the CTE program [4].

It is proposed that a macro-scale material model can be used to accurately predict failure in plain-weave fabric composite laminates. This work seeks to investigate the capabilities of a model using finite elements, failure criteria, and post-damage behavior to capture the failure of woven composite laminates under tensile loading conditions. Each of the following objectives will be met:

1. Implement a material model in Abaqus, a finite element solver, as a user-defined subroutine. The material model will use orthotropic and plane-stress assumptions to calculate stress.
2. Select a failure criteria that best represents plain-weave composite materials.
3. Develop a post damage model that predicts the material's behavior after damage occurs.
4. Validate the model for notched and unnotched geometries using material data from NIAR [4].

Several steps were taken in developing the model. First, the material model was validated against material data for the case of the linear stress-strain curve. This was done for individual plies and then a laminate. Failure criteria was introduced which reduced the stresses to zero upon being reached. A post-damage behavior model was developed. Instead of having stresses reduced to zero, the stresses were now reduced to a fraction of the failure stress until completely failing at a later specified strain value. With a completed framework for the model, several parameters were adjusted in the analyses. Three failure criteria were investigated and an array of post damage parameters were tested. This model and all combinations of parameters were tested using a single material, a specific sixteen ply laminate layup, and two coupon geometries. The combination of material model parameters that provided results closest to the desired outcome was tested against two more laminate layups to further verify the results.

Physical testing of woven composite laminates was set to take place at NASA Langley and the results to be used in validating the work in this thesis. Unfortunately, the testing was rescheduled and it became infeasible to include validation within the timeframe of this thesis.

This thesis is divided into six chapters, the first of which is the introduction. The literature review covers research relevant to failure criteria and damage approaches for composites. Chapter three describes the finite element model and the choices that were made to develop it. Chapters four and five present the damage model and the results of each. The final chapter compares a chosen damage model to two new layups and draws conclusions from the results.

2 LITERATURE REVIEW

Lightweight high strength composites have become very common in the aerospace industry. Extensive testing is often required to properly characterize a composite structure for real applications in practice. Due to the high expense associated with experimental testing, significant research has been done to develop analytical models that can predict the behavior of composite material. Because of the many different uses of composites and the varied forms in which composites are used, modeling composites is a broad spectrum of research. The focus of this thesis is the failure of woven fabric composites. Areas of research most relevant to this topic include macro-level damage initiation and post-damage models for composites.

2.1 Failure Criteria-Based Approach for Composites

Composite damage models can be grouped by the scale at which damage is predicted. Macro scale models assume composite layers to be homogenous and orthotropic whereas meso-scale and micro-scale models analyze the fiber and matrix as separate entities [5]. Macro-level models sacrifice fidelity for a faster and often more practical approach to predicting general failure behavior. While macro-level failure modeling includes topics such as the continuum damage-based approach and the plasticity-based approach [6], this report will focus on a failure criteria-based approach.

Failure criteria-based approaches are named as such because they establish a failure criteria based on either stress or strain. When the failure criteria is met, the onset of damage occurs. Some failure criteria-based approaches rely on a single criterion, which represents all of the failure modes collectively while others differentiate between different failure modes. Using these distinctions, failure criteria can be grouped into three categories: non-interactive, partially interactive, and fully interactive [7].

Numerous failure criteria have been developed over the years, each seeking to best predict the failure of composite materials. Multiple surveys [8, 9] have been conducted to test the most popular failure criteria against laminates of different layups and loading directions. The conclusion from these surveys was that while some failure criteria outperformed others, there was no clear best choice for all scenarios.

2.1.1 Non-interactive Failure Criteria

Non-interactive failure criteria are considered non-interactive because they assume that different failure modes are independent. This means that the stresses in one mode, such as tensile fiber failure, are not considered when determining failure in another mode, such as compression or shear. The Maximum Stress and Maximum Strain failure criteria are the simplest and most common non-interactive failure criteria.

For plane-stress, the Maximum Stress failure criterion states that failure will occur as soon as one or more of the following conditions is no longer true:

$$\sigma_{1T} \geq \sigma_{1T}^{u},\ \ \sigma_{1C} \geq \sigma_{1C}^{u},\ \ \sigma_{2T} \geq \sigma_{2T}^{u},\ \ \sigma_{2C} \geq \sigma_{2C}^{u},\ \ \sigma_{12} \geq \sigma_{12}^{u} \tag{2.1}$$

Equation 2.1 Maximum Stress failure criteria [10]

The strength of whichever material is being analyzed is found experimentally for each direction. Whichever condition in Equation 2.1 is satisfied first determines the mode of failure. Failure modes for the Maximum Stress failure criteria include tension and compression along the first and second principal axes as well as in shear. For example, if σ_{1T} surpasses σ_{1T}^{u}, the composite is said to have failed in tension along the first principal axis. It is important to state that the criteria for each failure condition is independent from another. The failure criteria does not consider any combination of the stresses in the principal directions or shear when asserting that failure has been predicted.

A version of the Maximum Stress theory was presented by Zinoviev [11] in the survey by Hinton et al [8]. The failure criteria performed reasonably well in predicting the failure for unidirectional and multidirectional composites. Maximum Stress Theory was found to overestimate the lamina strengths at certain loading conditions but overall it was considered one of the best failure criteria available.

The Maximum Strain failure criteria is similar to the Maximum Stress failure criteria except that the stresses are replaced with their respective strains. Under the Maximum Strain failure criteria, failure will occur through plane-stress if any of the following conditions are no longer true:

$$\varepsilon_{1T} \geq \varepsilon_{1T}^{u},\ \ \varepsilon_{1C} \geq \varepsilon_{1C}^{u},\ \ \varepsilon_{2T} \geq \varepsilon_{2T}^{u},\ \ \varepsilon_{2C} \geq \varepsilon_{2C}^{u},\ \ \varepsilon_{12} \geq \varepsilon_{12}^{u} \tag{2.2}$$

Equation 2.2 Maximum Strain failure criteria [10]

Again, the strain limits are determined experimentally and each failure condition is independent from one another. The shear strains will not affect the failure conditions associated with a failure mode along the first or second principal axes.

From the survey of failure criteria by Hinton et al., the Maximum Strain theory was determined to be nonconservative and one of the less applicable failure theories [8]. The criteria struggled to predict failure under biaxial tensile and compression loading. Hart-Smith concluded that what the theory lacked most was the inclusion of nonlinearities in stress/strain curves [12].

While the Hinton survey focused on unidirectional and multidirectional laminates, other studies have focused on woven composites. Wang and Socie conducted biaxial loading tests on G-10 woven composite laminates and found that the failure strain envelope was bounded by the uniaxial ultimate strains of the laminate, as predicted by the Maximum Strain and Maximum Stress criteria [13]. Zhao et al. compared Maximum Stress theory with a modified Maximum Stress theory to predict failure in woven composite pi joints. The modified Maximum Stress theory used Mohr circle theory to find the maximum principal stresses to determine matrix cracking and fiber matrix shear-out. The results from the simple Maximum Stress failure criteria agreed very well with the experimental results and compared favorably with the empirical results [14].

2.1.2 Fully-interactive Failure Criteria

Fully-interactive failure theories do not distinguish between failure modes. Unlike the Maximum Stress and Strain theories, failure is evaluated as a combination of factors. A single equation which takes into account stresses or strains from various directions is used to determine whether a material has failed or not. The most common fully-interactive failure theories for composite materials are the Tsai-Wu and Tsai-Hill methods [9].

The Tsai-Wu failure criterion is widely used for anisotropic composite materials, which have different strengths in tension and compression [15]. The failure theory uses material ultimate strength parameters, which consist of a material's strength in different directions $(\sigma_{1T}, \sigma_{1C}, \sigma_{2T}, \sigma_{2C}, \sigma_{12})$. The material strength parameters are used in conjunction with the

stresses experienced by the composite to produce a single value called the failure index. The material is said to have failed when the failure index reaches the value of 1. The general form of the Tsai-Wu criterion can be simplified for the plane-stress case, Equation 2.3.

$$F_1\sigma_1 + F_2\sigma_2 + F_{12}\sigma_1\sigma_2 + F_{11}\sigma_1^2 + F_{22}\sigma_2^2 + F_{66}\sigma_6^2 \geq 1,$$
$$F_1 = \frac{1}{\sigma_{1T}^u} - \frac{1}{\sigma_{1C}^u}, \quad F_2 = \frac{1}{\sigma_{2T}^u} - \frac{1}{\sigma_{2C}^u}, \quad F_{12} = \frac{-1}{2\sqrt{\sigma_{1T}^u\sigma_{1C}^u\sigma_{2T}^u\sigma_{2C}^u}} \quad F_{11} = \frac{1}{\sigma_{1T}^u \cdot \sigma_{1C}^u}, \tag{2.3}$$
$$F_{22} = \frac{1}{\sigma_{2T}^u \cdot \sigma_{2C}^u}, \quad F_{66} = \frac{1}{\sigma_{12}^{u\,2}}$$

Equation 2.3 Tsai-Wu failure criterion reduced for plane-stress

The Tsai-Wu failure criterion was also featured in the Hinton et al. survey [8]. It is one of the most well known criterion, popular for its simplicity and mathematical basis. The theory has difficulty predicting laminate failure under biaxial compression loading as well as large shear deformations. It is very successful in predicting the final failure envelope and proved to be among the most accurate theories. Ahn et al. found that between Tsai-Wu and Yamada–Sun, the Tsai-Wu failure criterion most accurately predicted failure in unidirectional and woven composite for laminated joints on an aircraft control rod [16].

The Tsai-Hill criterion is similar to the Tsai-Wu criterion. Both use a failure index of 1 and take into account the stresses and strengths in the primary directions. Tsai-Wu has linear terms and Tsai-Hill is purely quadratic. The equation for Tsai-Hill in plane-stress is seen below in Equation 2.4.

$$\left(\frac{\sigma_1}{\sigma_1^u}\right)^2 + \left(\frac{\sigma_2}{\sigma_2^u}\right)^2 - \left(\frac{\sigma_1\sigma_2}{\sigma_1^{u\,2}}\right) + \left(\frac{\tau_{12}}{\tau_{12u}}\right)^2 = 1 \tag{2.4}$$

Equation 2.4 Tsai-Hill failure criterion for plane-stress [17]

In a report by the US Department of Transportation, it concluded that the Tsai-Wu criterion was preferred over the Tsai-Hill criterion based on its success in matching test data [9]. Zahari et al. employed a progressive damage model that utilized the Tsai-Hill failure criterion to examine woven glass/epoxy composite laminated panels [18]. The progressive damage model was found to be in reasonable agreement with the experimental results.

2.1.3 Partially Interactive Failure Criteria

Partially interactive failure criteria distinguish between failure modes and use various stresses or strains to evaluate failure for each. Partially interactive methods differ from non-interactive methods in that multiple stresses or strains contribute to the failure of a particular mode as opposed to a single stress or strain. These theories hold the advantage that failure can be attributed to a particular mode without ignoring the combination of stresses or strains that may cause it. The Hashin and Puck failure criterion are both examples of partially interactive failure theories [19, 20].

The Hashin failure criterion distinguishes between two failure modes: fiber failure and matrix failure. A lamina is determined to have failed when the stress in the fiber direction reaches the strength of the lamina in the fiber direction. The matrix is determined to have failed when a combination of stresses in the matrix direction and shear stress reach 1. These criteria are shown below in Equation 2.5.

$$\left(\frac{\sigma_{1T}}{\sigma_{1T}^{u}}\right)^2 + \left(\frac{\sigma_{12}}{\sigma_{12}^{u}}\right)^2 \geq 1, \qquad \left(\frac{\sigma_{2T}}{\sigma_{2T}^{u}}\right)^2 + \left(\frac{\sigma_{12}}{\sigma_{12}^{u}}\right)^2 \geq 1 \tag{2.5}$$

Equation 2.5 Hashin failure criterion for a lamina

A version of the Hashin failure criterion was applied to the specimens in the Hinton survey where it performed at the lower end of failure theories. Its weakness was attributed to its handling of the response post initial failure [8]. Warren et al. proposed a progressive damage model for single-bolt, double-shear joints that utilized the Hashin failure criteria for damage initiation. It was concluded that the progressive damage model predicted experimental data reasonably well for the stress/strain behavior and failure modes [21]. Feng et al. also proposed a progressive damage model for woven composites using the Hashin failure criteria and found the experimental data to be in good agreement [22].

The Puck failure criterion consists of two independent paths for failure: fiber failure (FF) and inter-fiber failure (IFF). Fiber failure is determined in the same way as the Maximum Stress method. For inter-fiber failure, there are three failure modes. Each is determined by a combination of stresses, strengths, and material parameters. The modes indicate different failure mechanisms. Mode A failure is caused by the transverse tensile stress, Mode B failure is caused

by in-plane shear stress, and Mode C failure is caused by transverse compressive stress. The final equations for the failure criteria can be seen in the paper by Puck and Schurmann [23].

The Puck failure criterion was also included in the Hinton survey [8]. Compared to the other failure criterion, Puck had the most sophisticated method for predicting matrix cracking. The theoretical failure envelopes agreed very well with the experimental results for unidirectional laminae and were generally good for multidirectional laminates. It had trouble with large nonlinear deformations but overall the authors concluded it to be one of the best failure theories available.

2.2 Post-Damage Models for Composites

Failure criteria can be used as a damage model on its own but more often it is used to determine the initiation of damage. How the material behaves after damage is initiated is referred to as post-damage behavior. When the material is damaged, its properties are degraded [24]. The material may lose stiffness and strength. To predict post-damage behavior, post-damage models are created to handle the degradation of properties and the damaged material behavior. Post-damage models can range from simple implementations such as the ply discount method to more complex models which incorporate damage into continuum damage approaches.

The ply discount method is a simple and very conservative method that effectively removes the failed ply from any future calculations. Chu and Sun [25] proposed a failure analysis method that utilized the ply discount method and included free edge effects for composite laminates containing a center hole. Pal and Ray [26] implemented the ply discount method in finite element analysis to examine laminated composite plates under transverse static loading. This approach works in laminated plate theories because even after removing an entire failed ply, the laminate stiffness matrix is still diagonally dominant. It is generally observed that the ply-discount method underestimates laminate strength and stiffness because it does not recognize that the damage is localized and that a failed ply may have residual load-carrying capability [27].

In the ply discount method, the stiffness values of the failed plies are set to zero. This framework can be altered to set the stiffness values of failed plies to something other than zero. In simple post-damage models, the stiffness is reduced by a factor between zero and one of the original stiffness. However, there are many ways to go about reducing the stiffness of a failed

ply. Reddy et al. [30] proposed a stiffness reduction scheme in which stiffness properties of failed elements were reduced gradually resulting in partial unloading for an amount of damage. Cousigné et al. [28] investigated four post-damage definitions in application to woven composite laminates for crash simulations. These post-failure models were implemented in LS-DYNA as user-defined composite material models. They included linear damage, nonlinear damage, constant stress level, and step-based material degradation. Examples of these post-damage models are depicted in Figure 2.1. Cousigné et al. found all four of the post-damage models to have similar damaged areas that were in good agreement with the experimental results.

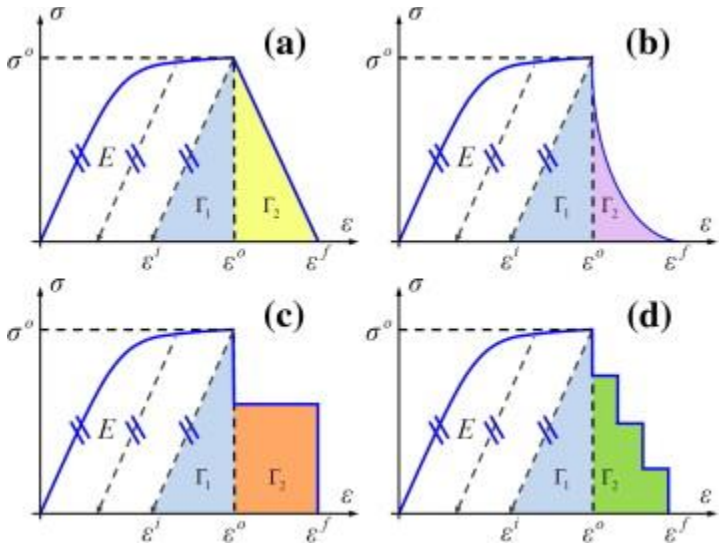

Figure 2.1 Post-damage models for woven composites: (a) Linear, (b) Nonlinear, (c) Constant stress level, and (d) step-based material degradation

Lastly, more complex post-damage models utilize continuum damage mechanics (CDM). As opposed to some of the more heuristic damage approaches, CDM models are based on irreversible thermodynamic processes. As an example of a CDM-based post-damage model, Okabe et al. [29] proposed a model for predicting the stiffness reduction of composite laminates which included transverse cracks formulated as a function of crack density. Damage variables were derived by assuming a plane strain field in the isotropic plane and using the Gudmundson–Zang model [30] as a comparison. The strain equivalent principle proposed by Murakami et al. [31] and classical laminate theory was used to formulate the elastic moduli of laminates of arbitrary lay-up configurations as a function of the damage variable. Okabe et al. found that although the model only considered the damage of the transverse crack, it seemed to be effective in the early stage of damage formation, when transverse cracking was the dominant failure mode.

3 LAMINATE FINITE ELEMENT MODEL

3.1 Laminate Properties

For this work, the analysis will be based off composite material data provided by NIAR [4]. The composite laminates consist of Hexcel 8552 - AS4 plain weave fabric. The material properties were obtained by testing warp and fill plies separately using ASTM D3039-00 and ASTM D3518. For each property, at least nineteen specimens were tested and the minimum, maximum, and average of each property was provided. The mean values for the relevant material properties are shown in Table 3.1.

Table 3.1. Ply level properties of Hexcel 8552 - AS4 plain weave fabric

Property	Value
Warp Tensile Modulus	65 GPa
Warp Compression Modulus	60 GPa
Warp Tensile Strength*	752 MPa
Warp Compression Strength*	794 MPa
Fill Tensile Modulus	66 GPa
Fill Compression Modulus	60 GPa
Fill Tensile Strength*	742 MPa
Fill Compression Strength*	752 MPa
Poisson's Ratio (Laminate)	0.3
Shear Modulus	(Values from curve)
Shear Strength*	84 MPa
Laminate Density	1600 kg/m^3

* Ultimate strength

There are six categories of laminate; each consists of 15-20 plies. Each ply is approximately 0.0078 in. thick and the laminates are approximately 37% resin by weight and 55% fiber by volume. The prepreg is a high strength structural epoxy matrix. For half of the laminates, there is a 0.25 in. notch (hole) in the center. The details of each category are shown in Table 3.2.

Table 3.2. Laminate layups for all cases

Case No.	Ply Layup	Notched
1	$[45/0/-45/90]2s$	No
2	$[45/-45/0/45/-45/45/-45/90/45/-45]s$	No
3	$[0/90/0/45/90/0/90/-45/90/0/90/45/0/90/0]$	No
4	$[45/0/-45/90]2s$	Yes
5	$[45/-45/0/45/-45/45/-45/90/45/-45]s$	Yes
6	$[0/90/0/45/90/0/90/-45/90/0/90/45/0/90/0]$	Yes

The dimensions were consistent for each laminate coupon. The laminate coupons were 6 in. in length, excluding the tabbed section, and 1.5 in. in width. When a notch was present, it was centered and had a 0.25 in. diameter. The laminate dimensions are shown in Figure 3.1.

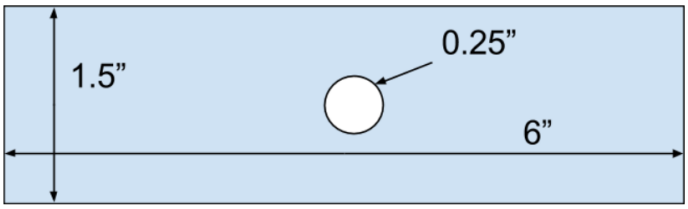

Figure 3.1. Laminate measurements provided by NIAR [4]

3.2 Finite Element Model

In developing a method to predict damage in woven composites, a finite element model (FEM) will be used to apply the failure criteria and post-damage behavior. A finite element model is different from classical laminate analysis in that the model can be discretized into elements where stress, strain, and failure calculations can be applied to each element. By discretizing complex geometries into smaller more uniform elements, the complex geometries can be analyzed without oversimplifying features. While a finite element approach is useful and often necessary for more complex problems, an analytical tool such as the ply-discount method can be used to as a first step into analyzing simpler geometries. For the unnotched case, a single

element analysis was performed to ensure the finite element model was correctly predicting stress.

The finite element model was developed for each laminate case using Abaqus. Shell elements (S4R) were used in modeling the laminate. The through-thickness stresses and strains (S33, S13, S23, E33, E13, and E23) were not considered for this work because the layups are balanced and the tests apply in-plane loads rather than normal loads. Using shell elements as opposed to solid elements also decreases computation time. The composite layup tool within Abaqus CAE was used to create the various layups. The geometry reflected the dimensions of Figure 3.1 and the constraints were assigned to replicate a tension test. While various shapes were considered for the Abaqus model, including a "dog bone" shape, it was decided that no change to the geometry was necessary. Any stress concentrations that may occur in the unnotched laminate due to boundary conditions could be worked around from within Abaqus. For example, the stress concentrations that formed at the left and right ends of the unnotched laminate were ignored in the failure calculations made by the user-defined subroutine.

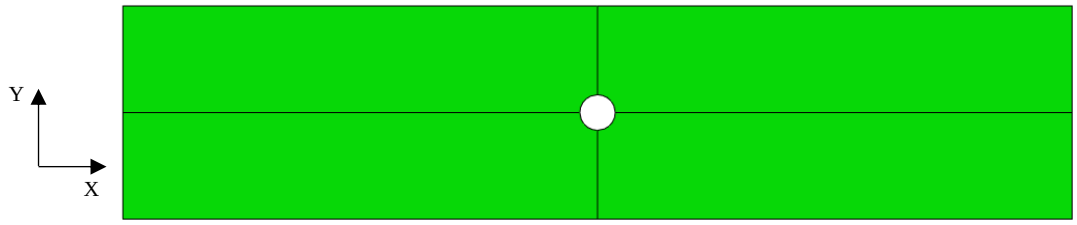

Figure 3.2. Notched laminate geometry modeled in Abaqus/CAE

3.2.1 Boundary Conditions and Loads

The notched and unnotched geometries were constrained along the left and right vertical edges. The constraint on the left edge was fixed translationally and rotationally in the x, y, and z directions. The constraint on the right edge was also fixed translationally and rotationally in the x, y, and z directions but the transitional x displacement was incremented with positive displacement until failure occurred. A reference node was placed to the left of the geometry and was used to capture the reaction force of the constrained left edge. No other constraints or loads were placed on the model.

Table 3.3 Boundary Conditions and Loads

BC 1 - left edge	TX, TY, TZ, RX, RY, RZ
BC 2 - right edge	TX (incremented displacement), TY, TZ, RX, RY, RZ

3.2.2 Determining Mesh Size

Mesh size can significantly affect a model's results. If the elements are too large or if there is a stress concentration present, changing the element size will produce different stress and strain values. A mesh refinement study was performed to determine the element size. Figure 3.3 details the behavior of the stress results with changing mesh size. The data was taken from an element at the center of an unnotched laminate geometry for a quasi-isotropic laminate with an applied end displacement. The material properties from Table 3.1 were used.

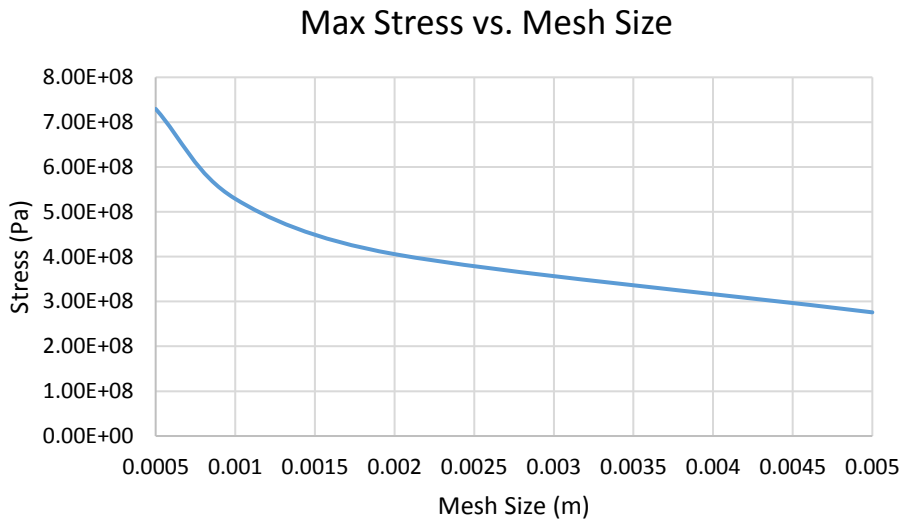

Figure 3.3. Mesh refinement study for notched laminate

Apparent from Figure 3.3, a feasible range of mesh sizes, the mesh does not converge to a mesh independent result. This means that for the current model, mesh size will always affect the results to some degree. This is the result of using a linear stress model that ignores plastic effects. If some elements were able to plastically deform, the stress singularity would redistribute the

load over a larger number of elements and the model may then be considered stable. However, within the scope of this work, the composite laminates were considered brittle enough that any benefits of implementing a plastic behavior model would be insignificant. Without a plastic behavior model, a mesh dependent mesh size must be chosen.

Using a linear shell-based finite element model for laminate composites has been shown to be mesh dependent even with the inclusion of a damage model [32]. Satyanarayana proposed that this could be avoided by selecting a baseline mesh size and scaling the effects using data from physical test results. An intermediate point is to be selected at which the magnitude of the derivative curve reaches zero indicating a constant failure load. A plot for several quasi-isotropic laminates is shown in Figure 3.4.

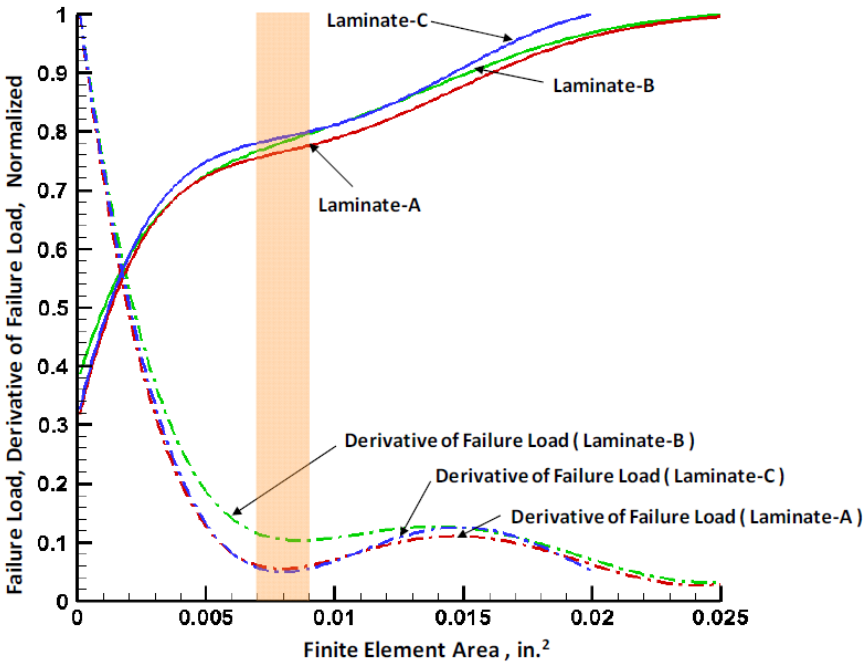

Figure 3.4. Normalized failure load and derivatives with respect to element area

Based on Satyanarayana's results, an element size of 4E-6 m^2 (0.0062 in^2) was selected. This element size captures the features of the geometry while using Satyanarayana's element size as a starting point. While mesh convergence is a point that will need further investigation, consistency with previous work will be prioritized for this thesis. This element size will be maintained throughout the remainder of this work to form consistent results. If physical data is

later obtained, the results can be extended for different element sizes. Figure 3.5 shows the geometry model meshed with the chosen element size.

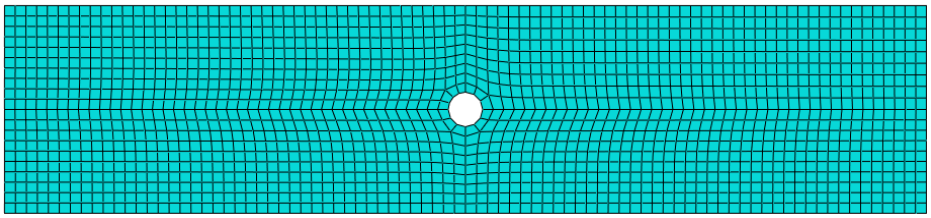

Figure 3.5. Laminate model using selected mesh size

Another consideration in choosing this element size was computation cost. A goal of this work is to develop a damage model that can be used to aid in making design decisions. A model that can be effective while running multiple times a day is of more use than one which takes multiple days and provides extraneous information.

3.2.3 Running Explicit Analysis

Abaqus/Standard offers an implicit solver that is capable of receiving user-defined subroutines (UMATs). These UMATs allow custom materials and element behaviors to be defined. It does not however have the ability to delete elements that are marked as failed. For this reason Abaqus/Explicit, an explicit solver, will be used instead. Explicit solvers are typically used for dynamic problems as they excel at nonlinear solutions. While a tension test is not necessarily a dynamic problem, Abaqus/Explicit will be able to capture the details of the laminate as it reaches failure. Abaqus/Explicit also accepts user-defined subroutines that are called VUMATs. Due to the flexibility of user-defined subroutines, a VUMAT will be used in place of the predefined damage models within Abaqus. One drawback of Abaqus/Explicit is the inability to use certain element types. Because this analysis uses shell elements, it will be limited to the S4R element formulation. S4R elements are a reduced-order integration shell element that consists of four nodes and one integration point in the center. This element type should be suitable for this work as it is consistent with previous work and performs well for large-strain analysis and tends to give more accurate results than other element types (provided the elements are not distorted or loaded by in-plane bending) [33].

3.2.4 Creating the VUMAT

Abaqus/Explicit analyzes a model by iteratively processing every material point over the course of many steps. Variables such as stress, strain, and displacement are unique to each material point. A VUMAT can be used to control exactly how Abaqus calculates these variables as well as creating new variables. The VUMAT is called at the beginning of every analogous time step. The structure of the VUMAT for this model can be represented by the flowchart in Figure 3.6.

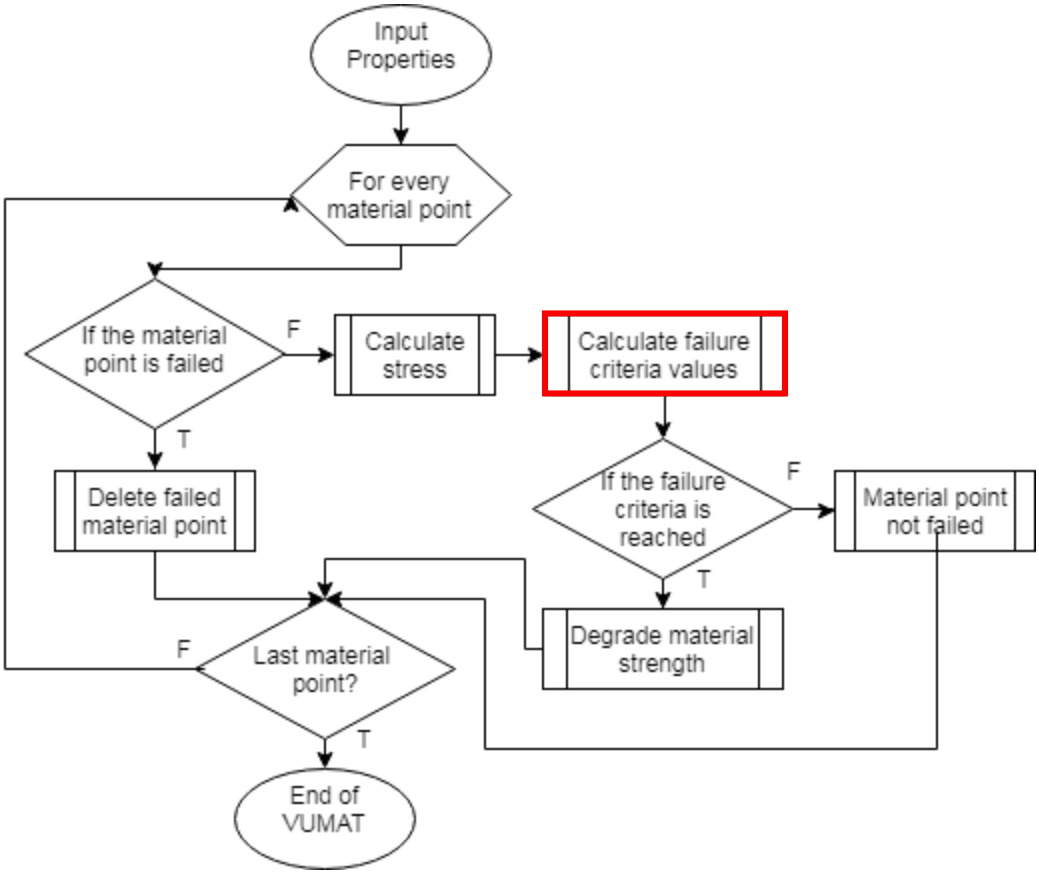

Figure 3.6. VUMAT flowchart for composite model

Each process is executed as an independent subroutine. This allows individual processes to be altered. For example, the subroutine for “failure criteria 1” can easily be swapped with the subroutine for “failure criteria 2” without affecting other aspects of the VUMAT.

Stress is calculated using plane-stress assumptions. Hooke's law for a plane-stress orthotropic material is shown in Equation 3.1 [34].

$$\begin{bmatrix} \sigma_{xx} \\ \sigma_{yy} \\ \sigma_{xy} \end{bmatrix} = \frac{1}{1-\nu_{xy}\nu_{yx}} \begin{bmatrix} E_x & \nu_{yx}E_x & 0 \\ \nu_{xy}E_y & E_y & 0 \\ 0 & 0 & G_{xy}(1-\nu_{xy}\nu_{yx}) \end{bmatrix} \begin{bmatrix} \varepsilon_{xx} \\ \varepsilon_{yy} \\ 2\varepsilon_{xy} \end{bmatrix} \quad (3.1)$$

Equation 3.1. Stress-strain relationship for orthotropic materials in plane-stress

Equation 3.1 is used to calculate the first two stress terms however shear stress is calculated using experimental data. The shear modulus was shown to be significantly nonlinear. The shear stress vs. shear strain plot from [4] is presented in Figure 3.7.

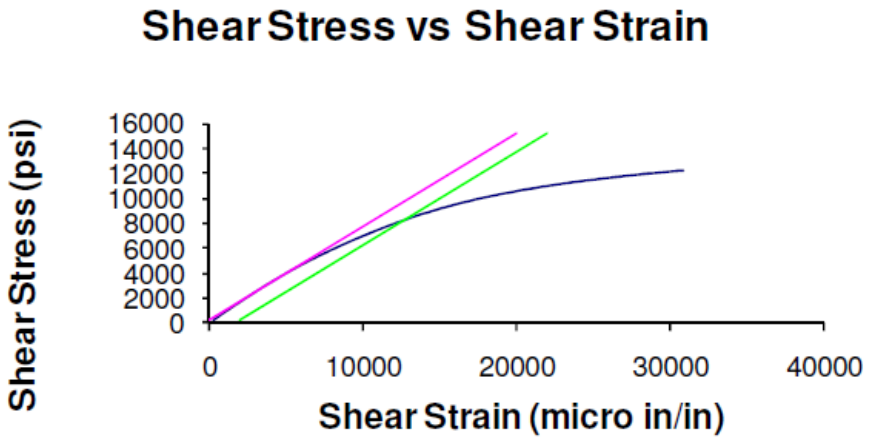

Figure 3.7. Shear stress vs. shear strain plot for AS4 plain weave

From the data a curve of degree three best fit, Equation 3.2, was created to approximate the shear modulus as a function of shear strain. In the case of a negative shear strain, the absolute value of the shear strain was used and the resulting shear stress was assigned a negative sign. Shear strains that exceeded the shear limit were assigned a large shear stress meant to trigger any failure criteria.

$$\tau_{12} = (1E12)\gamma_{12}{}^3 - (2E11)\gamma_{12}{}^2 + (6E9)\gamma_{12} + 24295 \quad (3.2)$$

Equation 3.2. Shear stress as a function of shear strain

Stress concentrations were developed at the ends of the specimen due to gripping the specimen. For the notched specimen this was not an issue because the stresses around the notch were much greater than the stress at the ends. However, they did cause elements at the end of the

unnotched specimen reached failure due to the stress concentrations when the rest of the specimen was still at a relatively low level of stress. The relative stress contour levels are plotted in Figure 3.8.

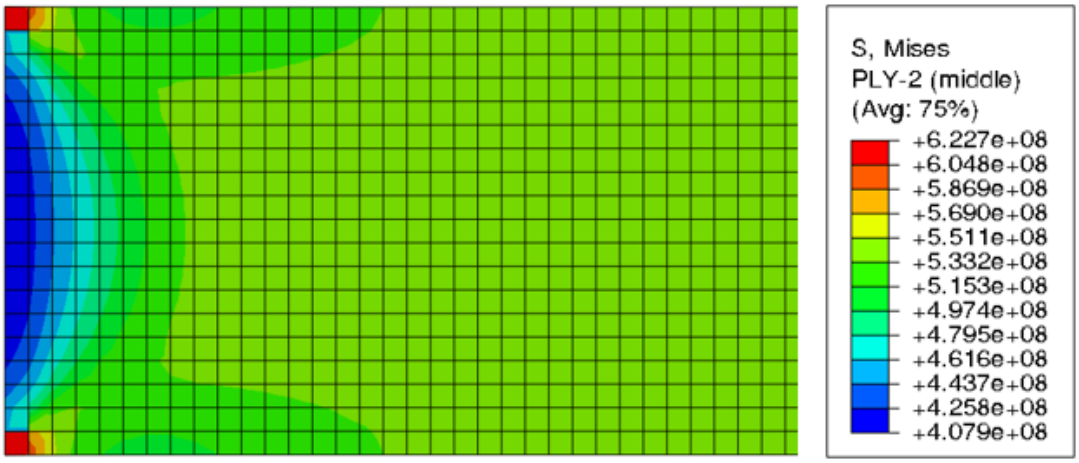

Figure 3.8. Stress concentrations at the ends of the unnotched specimen

The stress concentrations prevent the analysis from predicting when the analysis will fail in a test environment. To circumvent this problem, the VUMAT was programmed to ignore elements close to the ends that may be affected by the stress concentrations. Applying this criterion caused the specimen to fail later, better replicating the physical tests.

4 FAILURE CRITERIA FOR WOVEN COMPOSITES

In this work, damage will be referred to as any degradation in a material's properties. A damage model will be defined as having two parts: damage initiation and post-damage. The damage initiation model will utilize selected failure criteria to interpret the stresses applied to the material and determine when damage will first occur. The post-damage model will then take over and reduce the applied stresses by some predetermined pattern as a function of strain. This chapter will cover the damage initiation model and the following chapter will introduce the post-damage model.

4.1 Selected Failure Criteria

Many of the existing failure criteria are phenomenological; they identify failure without describing the behavior of the material. Failure criteria have varying degrees of success and often perform better or worse under certain loading conditions or material types. While classical failure criteria have been studied extensively for application to unidirectional laminates, there is significantly less literature regarding woven composite laminates. The literature that does cover woven composites identifies the Hashin, Tsai-Wu, and Maximum Stress theories as acceptable choices [21, 22, 16, 13, 14]. Other failure criteria have found varying degrees of success but will not be covered within the scope of this work.

The failure criteria to be considered are listed with their definitions below in Table 4.1. They are among the most popular of the classical failure criteria and initiate failure using different approaches. In most cases, these criteria can be applied to three-dimensional materials. In order to simplify the model and deal with the unavailability of certain material properties, the failure criteria will be reduced to the orthotropic plane-stress case. Reducing a composite model to the orthotropic plane-stress case has been successfully shown to compare well with experimental data in multiple studies [7, 9, 11, 16]. The plane-stress assumption is valid here as the stresses in the plane of a laminate will be much larger than those perpendicular to the plate [35] therefore an orthotropic plane-stress material model will be used. Another important assumption made is the smearing of the fiber and matrix properties. Rather than analyzing the fiber and matrix stresses and strains separately, they are smeared together as a homogenous orthotropic material. The smeared fiber-matrix property assumption is the foundation for most

macro-scale composite analyses. By smearing the fibers and matrix properties, structural applications can be modeled and analyzed with less computational expense [35].

Table 4.1. Selected failure criteria by name and criterion

Name	Failure Criteria
Tsai-Wu	$F_1\sigma_1 + F_2\sigma_2 + F_{12}\sigma_1\sigma_2 + F_{11}{\sigma_1}^2 + F_{22}{\sigma_2}^2 + F_{66}{\sigma_6}^2 \geq 1$ $F_1 = \frac{1}{\sigma_{1T}^u} - \frac{1}{\sigma_{1C}^u}$, $F_2 = \frac{1}{\sigma_{2T}^u} - \frac{1}{\sigma_{2C}^u}$, $F_{12} = \frac{-1}{2\sqrt{\sigma_{1T}^u \sigma_{1C}^u \sigma_{2T}^u \sigma_{2C}^u}}$, $F_{11} = \frac{1}{\sigma_{1T}^u \cdot \sigma_{1C}^u}$, $F_{22} = \frac{1}{\sigma_{2T}^u \cdot \sigma_{2C}^u}$, $F_{66} = \frac{1}{{\sigma_{12}^u}^2}$
Maximum-Stress	$\sigma_{1T} \geq \sigma_{1T}^u$, $\sigma_{1C} \geq \sigma_{1C}^u$, $\sigma_{2T} \geq \sigma_{2T}^u$, $\sigma_{2C} \geq \sigma_{2C}^u$, $\sigma_{12} \geq \sigma_{12}^u$
Hashin	$\left(\frac{\sigma_{1T}}{\sigma_{1T}^u}\right)^2 + \left(\frac{\sigma_{12}}{\sigma_{12}^u}\right)^2 \geq 1$, $\frac{{\sigma_{2T}}^2}{{\sigma_{2T}^u}^2} + \frac{{\sigma_{12}}^2}{{\sigma_{12}^u}^2} \geq 1$

4.2 Finite Element Results for Different Failure Criteria

The various failure criteria were incorporated into VUMATs and run under the same conditions for a notched and unnotched laminate with layup $[45/0/-45/90]2s$ (cases 1 and 4). The reaction force of BC 1 (from Table 3.3) was plotted against the displacement of BC 2 in the x-direction, Figure 4.1.

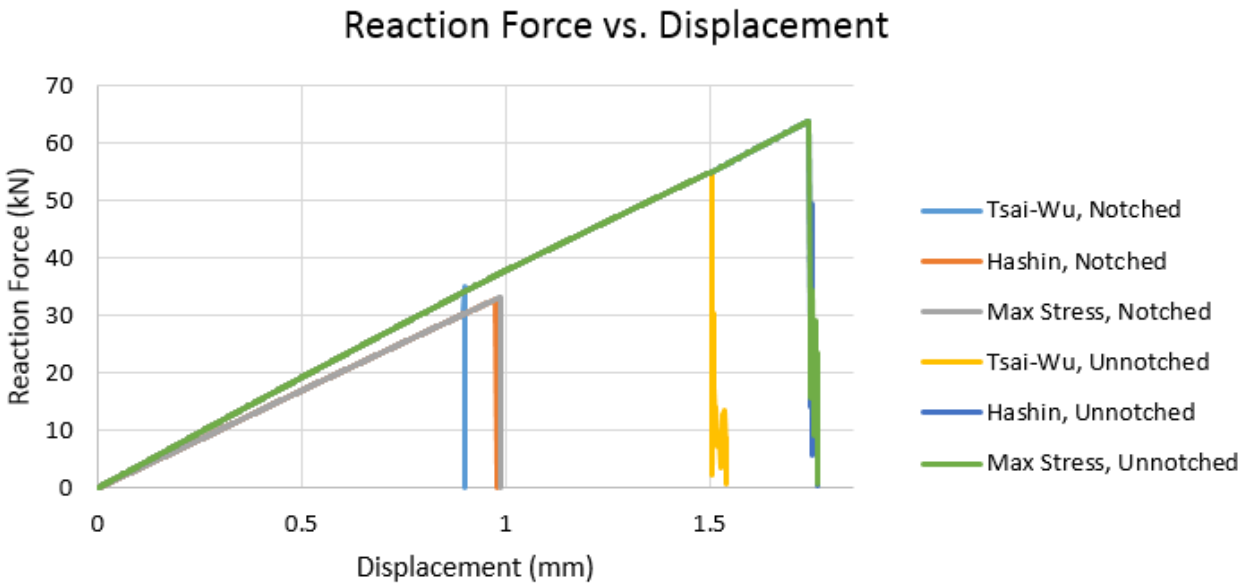

Figure 4.1. Force vs. displacement for each failure criteria, layup: [45/0/−45/90]2s

Figure 4.1 shows that each failure criteria determines failure at a particular load and displacement. For both the notched and unnotched cases, the Hashin and Maximum Stress criteria impose failure at approximately the same displacement and some amount after Tsai-Wu. The notched and unnotched geometries create a unique stress/strain modulus with the unnotched case being predictably more stiff. The failure criteria all follow this modulus up until failure is initiated. The modulus is not perfectly linear because of the contribution of the nonlinear shear modulus. At failure, there is some instability. Each case quickly descends to a low stress value with the exception of the notched Tsai-Wu case. It experiences a sudden spike before immediately going to zero. This spike is attributed to a numerical instability caused by deleting elements and can be ignored. It is worth noting that within the resolution of the results, the first element to fail immediately caused all connecting elements to fail as well. The redistribution of stresses was too much for the surrounding elements resulting in catastrophic failure.

A numerical summary of the results is presented in Table 4.2. The reaction force, displacement, and stress were each recorded immediately before failure. Stress was calculated by dividing the reaction force by the models cross-sectional area. Stress was calculated this way to better compare with the experimental data that calculated stress in the same manner.

Table 4.2. Results summary for selected failure criteria

	Failure Criteria	Reaction Force (kN)	Displacement (mm)	Stress (MPa)
Unnotched	*(Physical Specimen)*	---	---	**578**
	Tsai-Wu	55.1	1.51	456
	Maximum Stress	63.9	1.74	529
	Hashin	63.9	1.74	529
Notched	*(Physical Specimen)*	---	---	**295**
	Tsai-Wu	30.3	0.90	301
	Maximum Stress	33.2	1.00	330
	Hashin	32.9	0.99	327

Table 4.2 shows that the Maximum Stress and Hashin criteria have similar results and the Tsai-Wu criteria has comparatively lower values in all categories. The unnotched case was under predicted (lower failure stress than physical specimen) by all criteria and the notched case was over predicted (higher failure stress than physical specimen) by all criteria. It is not clear which criteria performs best as each fails to closely predict failure for either the notched or unnotched case. Overall, the Tsai-Wu cases are more conservative compared to the Hashin and Maximum Stress cases.

During each analysis, the laminates undergo the same conditions until the selected failure criteria determines the first element has failed. The unnotched laminates experienced high states of stress throughout the laminate. When the first element failed, every surrounding element in that ply was very near failure. This resulted in catastrophic failure for all of the unnotched cases. This result is as predicted and provided confidence in the model.

The highest states of stress for the notched case were at the top and bottom of the hole, where a stress concentration was expected. Because the specimen was under tension in the longitudinal direction, stress concentrations form around the hole furthest from the longitudinal centerline. There is a large stress gradient around the hole. Reducing the mesh size would create a higher resolution between material points and potentially give a more accurate result. However, this is not implemented for the reasons stated in section 3.2.1.

4.2.1 Failure Criteria Results for Tsai-Wu

Tsai-Wu is considered an interactive failure criterion because it takes into account the interactions between stresses and strains acting on the lamina [36]. Although one stress component does not determine failure, the largest term can be considered to have the greatest contribution to a laminate's failure. For the case of the unnotched and notched laminates with layup [45/0/-45/90]2s, the element stresses and values for each Tsai-Wu term are shown in the following tables. These values are taken from the first element to fail, immediately before failing.

For the unnotched case, the boundary effects were ignored, resulting in a section with a uniform stress distribution. Because of this, many of the elements reached failure at the same time. The stress values in Table 4.3 were taken from a single element which represented the plies' state of stress.

Table 4.3. Unnotched: stress values before failure (Tsai-Wu)

Stress Component (MPa)	Plies: 45 / -45	Plies: 0 / 90
σ_{11}	229	641
σ_{22}	229	-183
σ_{6}	-46	0

Table 4.4. Unnotched: term values for the first elements to fail (Tsai-Wu)

Ply	$F_1\times\sigma_1$	$F_2\times\sigma_2$	$F_{12}\times\sigma_1\sigma_2$	$F_{11}\times\sigma_1^2$	$F_{22}\times\sigma_2^2$	$F_{66}\times\sigma_6^2$	Σ
45 / -45	0.00	0.00	-0.08	0.08	0.08	0.30	0.38
0 / 90	0.00	0.00	0.23	0.69	0.08	0.00	**1.00**

From Table 4.3, for the unnotched laminate, the term which initiated failure is $F_{11}\times\sigma_1^2$ for the 0° and 90° plies. Table 4.4, shows the 0° and 90° plies experienced high tensile stress in the 11 (longitudinal) direction and relatively high compressive stresses in the 22 (latitudinal) direction. The 0° and 90° plies have a very small Poisson's ratio but when used as 45° and -45°

plies the “apparent” Poisson’s ratio is significantly greater. As a laminate composed of both ply types, the 45° and -45° plies apply a compressive stress on the 0° and 90° plies in the 22 direction and the 0° and 90° plies apply a tensile stress on the 45° and -45° plies in the 22 direction. This compressive stress on the 0° and 90° plies paired with the tensile stress in the 11 direction are enough to initiate failure in these plies. The 45° and -45° plies are still not close to failing due to their comparatively low “apparent” modulus, however the unnotched laminate fails catastrophically immediately after first ply failure.

Under the Tsai-Wu failure criteria, the unnotched laminate failed at a considerably lower stress than the physical tests. A secondary analysis was conducted using fifteen 0° plies under the same tensile loading conditions and failure occurred at 751.9 MPa. The physical test results for this case list failure as 751.66 MPa. The analysis results matched within 0.1% of the physical test results. This indicates that the discrepancy is introduced with the 45° and -45° plies. It is possible that the issue has to do with the shear modulus or the elastic interlaminar properties for which this analysis assumes to be a perfectly bonded connection.

The notched case, unlike the unnotched case, is non-uniform and has a large stress concentration across the notch in the longitudinal direction. The von Mises stresses for the first (45°) and second (0°) plies are shown in Figure 4.2.

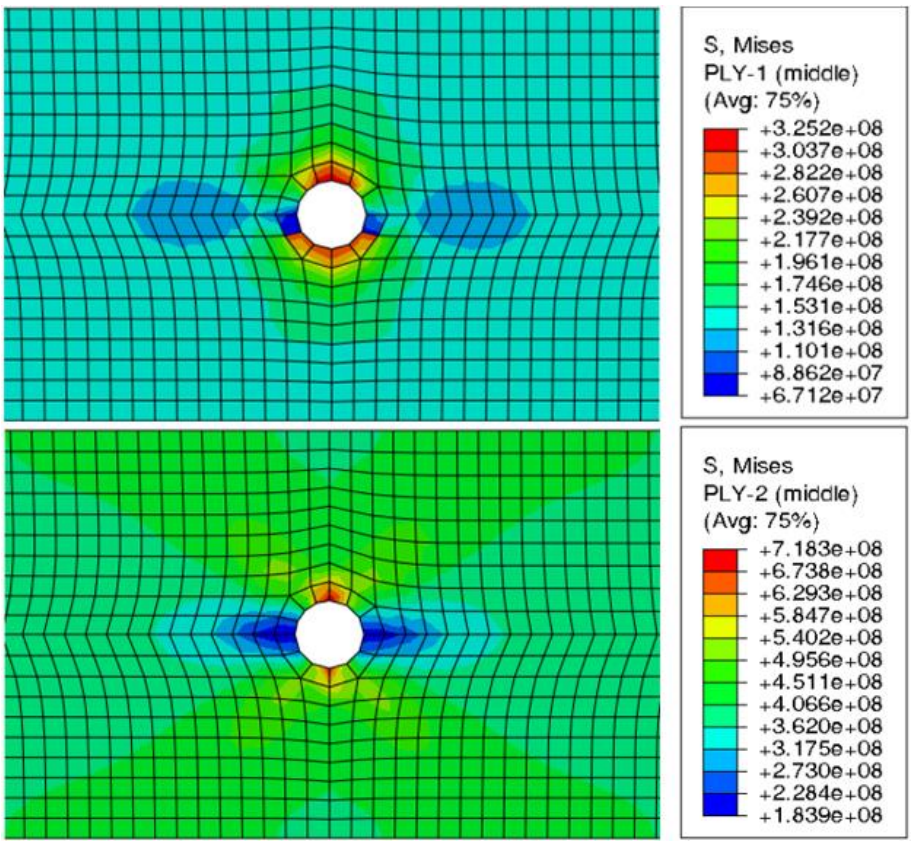

Figure 4.2. von Mises stresses (MPa) for the first and second plies (Tsai-Wu)

Table 4.5. Notched: stress values before failure (Tsai-Wu)

Stress Component (MPa)	Plies: 45 / -45	Plies: 0 / 90
σ_{11}	239	659
σ_{22}	270	-140
σ_{6}	45	15

Table 4.6. Notched: term values for the first elements to fail (Tsai-Wu)

Ply	$F_1 \times \sigma_1$	$F_2 \times \sigma_2$	$F_{12} \times \sigma_1 \sigma_2$	$F_{11} \times \sigma_1^2$	$F_{22} \times \sigma_2^2$	$F_{66} \times \sigma_6^2$	Σ
45 / -45	0.00	0.00	-0.11	0.10	0.13	0.29	0.40
0 / 90	0.00	0.00	0.16	0.77	0.03	0.03	**1.00**

Similar to the unnotched case, Table 4.6 shows that the laminate failed first in the 0° and 90° plies. The stress at which the notched model failed however was much closer to the physical specimen, possibly because of the mesh size around the hole. A closer look at the effect of element selection and/or mesh size may be necessary in future work.

4.2.2 Failure Criteria Results for Maximum Stress

The Maximum Stress failure criteria is a non-interactive stress criterion. Its state of failure does not depend on how the different stresses or strains interact. It simply checks if the directional stress has exceeded the directional strength. It is easier to detect which mode the laminate is expected to have failed because the values are independent. For the case of the notched and unnotched laminates with layup [45/0/-45/90]2s, the values for each term for the first element that failed, immediately before failing, are shown in the tables below.

As the case with using Tsai-Wu criterion, the boundary effects were ignored on the unnotched specimen leaving a uniform stress distribution across the center. An element that develops this state of stress was selected and the stress values and failure criteria terms are shown in Table 4.7 and Table 4.8.

Table 4.7. Unnotched: stress values before failure (Maximum Stress)

Stress Component (MPa)	Plies: 45 / -45	Plies: 0 / 90
σ_{11}	266	750
σ_{22}	266	-217
σ_{6}	-48	0

Table 4.8. Unnotched: term values for the first elements to fail (Maximum Stress)

Ply	$\sigma_{1T} \div \sigma_{1T}^{u}$	$\sigma_{2T} \div \sigma_{2T}^{u}$	$\sigma_{12T} \div \sigma_{12T}^{u}$
45 / -45	0.35	0.35	-0.57
0 / 90	**1.00**	-0.35	0.00

The 0° and 90° plies failed first due to tensile stress in the x-direction. This failure is similar to the Tsai-Wu results but because the Maximum Stress criterion considers stresses individually, failure occurred later. The failure stress for the unnotched laminate was still significantly lower, approximately 50 MPa less, than that of the physical specimen. This result means that for the Tsai-Wu case even if the stress in σ_{22} were zero, it would still predict failure much earlier than the physical specimen. Because the Maximum Stress model failed at lower stress values compared to the physical specimen, the 45° and -45° plies must be responsible for the discrepancy. If the analysis matches the physical test results well for the case of fifteen 0° plies, and the quasi-isotropic laminate fails early even when disregarding the influence from σ_{22} stresses, the remaining variables are the shear strength and shear modulus.

The notched results for the Maximum Stress failure criteria was similar to the notched Tsai-Wu results but had a higher failure stress. This is expected as the Tsai-Wu case was dependent on multiple stresses. The failure stress predicted by the finite element model using the Maximum Stress criterion was slightly higher than the physical results, Table 4.2. Failure was initiated by the 0° and 90° plies as a result of the σ_{1T} stresses at the top and bottom of the notch. The von Mises stresses for the first (45°) and second (0°) ply as well as the failure criteria stresses and terms are shown below in Figure 4.3, Table 4.9, and Table 4.10.

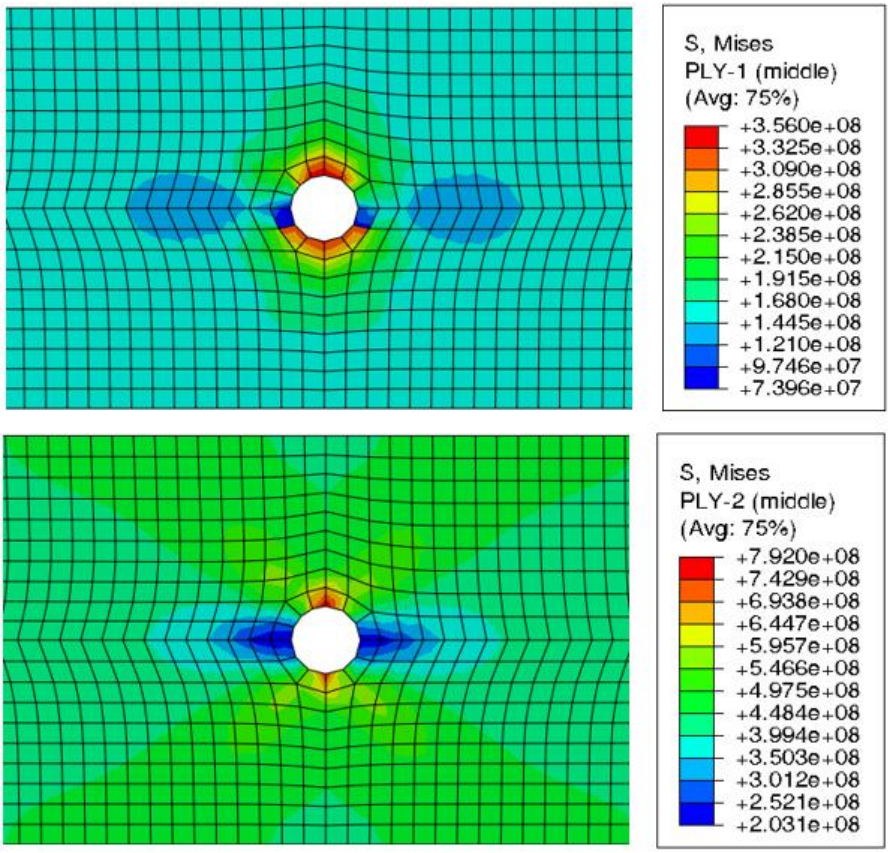

Figure 4.3. von Mises stresses (MPa) for the first and second plies (Maximum Stress)

Table 4.9. Notched: stress values before failure (Maximum Stress)

Stress Component (MPa)	Plies: 45 / -45	Plies: 0 / 90
σ_{1T}	299	750
σ_{2T}	334	-116
σ_{12T}	-48	-3

Table 4.10. Notched: term values for the first elements to fail (Maximum Stress)

Ply	$\sigma_{1T} \div \sigma_{1T}^{u}$	$\sigma_{2T} \div \sigma_{2T}^{u}$	$\sigma_{12T} \div \sigma_{12T}^{u}$
45 / -45	0.40	0.45	-0.57
0 / 90	**1.00**	-0.16	-0.03

The unnotched case continues to under predict the failure stress whereas the notched case has now over predicted failure. It is likely that some failure mechanism is not being represented correctly by the Maximum Stress failure criterion used by the model.

4.2.3 Failure Criteria Results for Hashin

Hashin, like Tsai-Wu, is an interactive stress criteria. Rather than having one all-encompassing equation to determine failure, the Hashin criterion considers two equations, one which handles stress in the longitudinal and shear directions and the other involves stress in the lateral and shear directions. The values for each term in both equations are shown in the following tables for the laminate with layup [45/0/-45/90]2s. The values in Table 4.11 were taken immediately before the first element failed.

Table 4.11. Unnotched: stress values before failure (Hashin)

Stress Component (MPa)	Plies: 45 / -45	Plies: 0 / 90
σ_{11}	266	750
σ_{22}	266	-217
σ_{6}	-48	0

Table 4.12. Unnotched: term values for the first elements to fail (Hashin)

Ply	$(\sigma_{1T}\div\sigma_{1T}^{u})^2$	$(\sigma_{12}\div\sigma_{12}^{u})^2$	Σ	$(\sigma_{2T}\div\sigma_{2T}^{u})^2$	$(\sigma_{12}\div\sigma_{12}^{u})^2$	Σ
45 / -45	0.13	0.33	0.46	0.13	0.33	0.46
0 / 90	1.00	0.00	**1.00**	0.08	0.00	0.08

The unnotched results for the Hashin failure criteria are very similar to those of the Maximum Stress failure criteria. The primary difference between the two criteria is the pairing of shear stress with a tensile stress in Hashin. Because the shear stress in the 0° and 90° plies is effectively zero, both failure criteria initiate failure at approximately the same load levels. As with the Maximum Stress case, the unnotched laminate using Hashin predicts failure before the failure of the physical specimen.

The notched results are also very similar between Hashin and Maximum Stress. Failure was initiated by the 0° and 90° plies because of the σ_{1T} stresses at the top and bottom of the notch. With a very low shear stress, the difference between the two criteria initiate failure is negligible. The von Mises stress plots of the first (45°) and second (0°) ply immediately before failure as well as the failure criteria terms are shown below in Figure 4.4, Table 4.13, and Table 4.14.

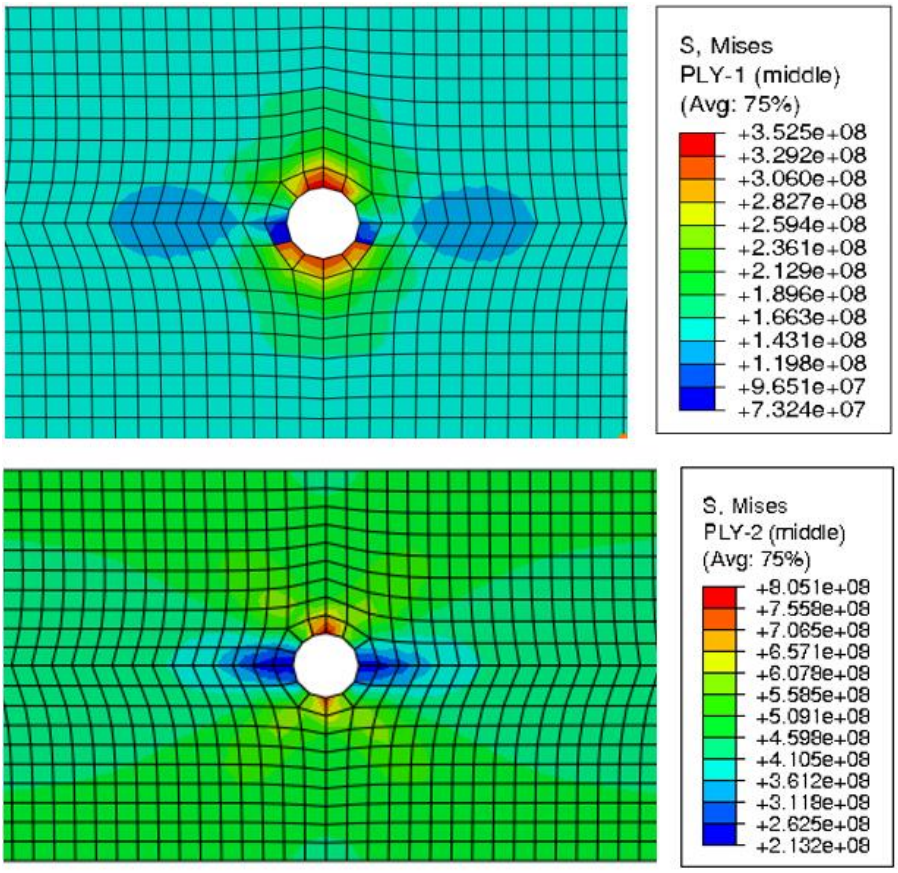

Figure 4.4. von Mises stresses (MPa) for the first and second plies (Hashin)

Table 4.13. Notched: stress values before failure (Hashin)

Stress Component (MPa)	Plies: 45 / -45	Plies: 0 / 90
σ_{1T}	300	750
σ_{2T}	334	-115
σ_{12T}	-48	-3

Table 4.14. Notched: term values for the first elements to fail (Hashin)

Ply	$(\sigma_{1T} \div \sigma_{1T}^{u})^2$	$(\sigma_{12} \div \sigma_{12}^{u})^2$	Σ	$(\sigma_{2T} \div \sigma_{2T}^{u})^2$	$(\sigma_{12} \div \sigma_{12}^{u})^2$	Σ
45 / -45	0.16	0.33	0.49	0.20	0.33	0.53
0 / 90	1.00	0.00	**1.00**	0.02	0.00	0.02

4.3 Failure Criteria Summary

The Tsai-Wu failure criteria predicted failure stresses that were relatively close to the physical specimen in the case of the notched laminate while the Maximum Stress and Hashin failure criteria predicted failure stresses that were closest to the unnotched laminate. Optimally the selected failure criteria would work well for both notched and unnotched laminates. To further examine the results, the ratios of the failure stresses were calculated relative to the failure loads of the physical specimen and presented in Table 4.15.

Table 4.15. Ratio of notched to unnotched failure stresses

	Failure Stress (MPa)		Notched/Unnotched Ratio
	Notched	Unnotched	
(Physical Specimen)	295	578	**0.51**
Tsai-Wu	301	456	0.66
Maximum Stress	330	529	0.62
Hashin	327	529	0.62

Table 4.15 shows that the while the Maximum Stress and Hashin criteria have a ratio most similar to the physical specimen, the ratios are still far from optimal. The Tsai-Wu ratio is not much further off and should still be considered. A similar ratio is desired because the addition of damage propagation can adjust the exact point of failure. The failure criteria used only predict the onset of failure. With the current model, material points that reach the onset of failure have their stresses reduced to zero. A damage propagation model can be used to manipulate stresses in material points after reaching the onset of failure. The addition of damage propagation to the material model may create a better compromise of the notched and unnotched failure stress in relation to the physical specimen.

5 POST-DAMAGE BEHAVIOR FOR WOVEN COMPOSITES

5.1 Model for Post Damage Behavior

When a failure criterion has been met it indicates that damage has been initiated for the material. How the material reacts to damage initiation is a major part of creating a complete damage model. Macro-scale damage models typically reduce the mechanical properties in some pattern to anticipate the material's behavior. In the case of a simple tension test, reducing a material's stiffness will have the greatest effect on its behavior. Several common variations of stiffness reduction are presented in Figure 5.1.

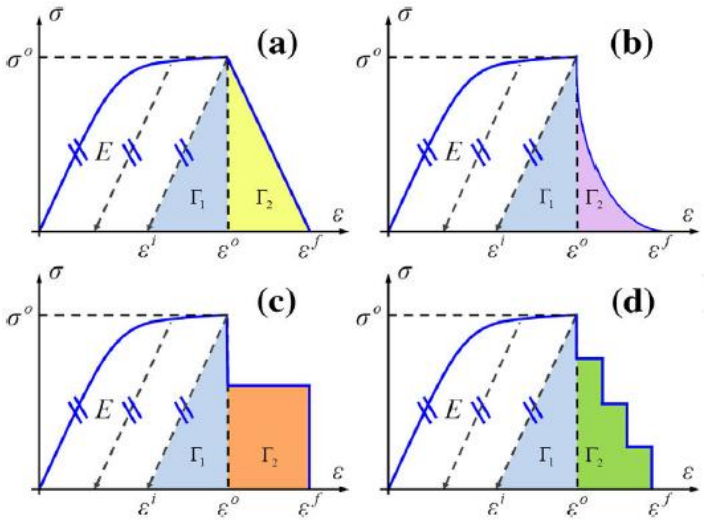

Figure 5.1. Four post-damage models for woven fabric materials: (a) linear damage, (b) non-linear damage, (c) constant stress level, (d) step-based material degradation [28].

Although each approach represents a material's post-damage behavior differently, the results from Cousigné et al. [28] show that the differences were not significant for the case(s) studied. Due to the similarity of the results, only the constant stress level pattern (c) will be implemented in this research. While from a physical perspective, the post-damage behavior of a woven composite may be more similar to Figure 5.1 (b), Figure 5.1 (c) should approximate the behavior well. The model in Figure 5.1 (c) was chosen because of its prevalence in existing damage models and its simplicity in implementation and manipulation.

For the damage model, the failure criteria will use stresses to determine when damage is initiated and strains will be used to determine when the element has completely failed. The two

parameters that make up the post-damage model are a failure strain term and a reduced stress term. Figure 5.1 shows the stress-strain curves ending at distinct failure strains. Because failure strains were not provided in the NIAR data or from laminate test results as a material property, the failure strain will be variable rather than fixed. Strain failure will be determined using a chosen percentage value multiplied by an initial strain failure value. The initial strain failure value was estimated by examining the strains at which various failure criteria were met. Two separate failure strain criteria are used: volumetric and shear. The volumetric strain, Equation 5.1, is measured by the sum of the strains in the fiber directions and the shear strain is simply the shear strain of the element.

$$\varepsilon_v = \varepsilon_x + \varepsilon_y + \varepsilon_z \tag{5.1}$$

Equation 5.1

Damage reduces a material's properties, most notably stiffness in the case of a simple tension test. Rather than degrade the stiffness, the VUMAT will directly degrade the state of stress when damage occurs by a reduced stress factor. This new state of stress will be kept constant until the failure strain criteria is met. An example of how the two variables can be manipulated is shown in Figure 5.2 and a numerical example for an arbitrary failure state is presented in Figure 5.3.

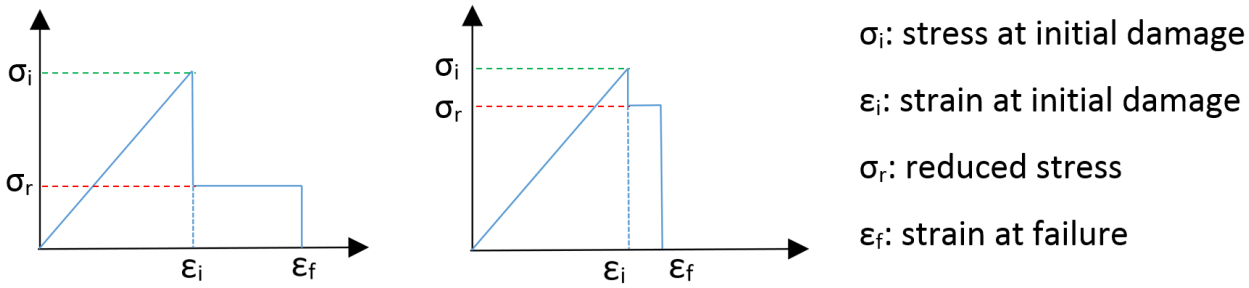

Figure 5.2. (Left) large failure strain, low reduced stress (right) small failure strain, high reduced stress

Chosen Parameters:

Failure Strain:	130%
Stress Degradation:	30%

Nominal Strain Limit:

Fiber Failure Strain:	$\varepsilon_{11} + \varepsilon_{22} = 0.0105$
Shear Failure Strain:	$\gamma_{12} = 0.0225$

Adjusted Strain Limit:

Fiber Failure Strain:	$\varepsilon_{11} + \varepsilon_{22} = 0.0195$
Shear Failure Strain:	$\gamma_{12} = 0.0293$

Stresses at Failure Criteria:

Warp	193 MPa
Fill	187 MPa
Shear	56 MPa

Stresses after Failure Criteria:

Warp	58 MPa
Fill	56 MPa
Shear	17 MPa

Figure 5.3. Changes in failure strain and stress for given parameters

A notable detail of the constant-stress-level model is that when failure occurs, the failure is not attributed to a particular direction. Unidirectional composites often consider matrix failure separately from fiber failure. While a more detailed model may be able to capture the effects of different failure modes, the constant-stress-level damage model will consider the intertwined fibers to be dependent on one another and will reduce strength uniformly.

5.2 Response Surface and Model Parameters

To determine which values are most appropriate for the post-damage model, a range of values for reduced stress and failure strain must first be established. The reduced stress must be some value between one and zero. A reduced stress range of 50% to 100% was chosen. The upper bound (100%) for this range was set such that the element will not be able to sustain any additional loading. While it is more common to degrade the stress, some damage models, such as the one proposed by Murray and L. Schwer, allow for additional loading [37]. The lower bound (50%) was chosen after several initial tests showed that the model would catastrophically fail under a reduced stress of 50% and lower unless the strain limit was greatly extended. For the failure strain range, test data was provided for failure in the shear direction but not for the fiber direction. It was assumed that a stiff material such as a fiber composite is not likely to reach high

levels of strain before its strength is significantly reduced. A range of 100% to 200% was selected for failure strain that should cover representative outcomes.

If each range for these two parameters is incremented by one percent, there are 5151 unique combinations for the damage model. Rather than test each case individually, a handful of cases will be selected using the Method of Low Discrepancy Sampling. The stress at catastrophic failure will be recorded and then a response surface can be created using least-squares regression. A quadratic polynomial model will be used for the response surface as it usually provides the best compromise between modeling accuracy and computational expense compared to the linear or higher order polynomial models [38]. The sampled data points and corresponding responses are denoted by Equation 5.2 and Equation 5.3Equation 5.3 where n is the number of data points and m is the number of variables.

$$S = \left[x^{(1)}, \dots, x^{(n)}\right]^T \in \mathbb{R}^m, \tag{5.2}$$

Equation 5.2

$$y_s = [y^{(1)}, \dots, y^{(n)}]^T = [y\left(x^{(1)}\right), \dots, y\left(x^{(n)}\right)]^T \in \mathbb{R}^n, \tag{5.3}$$

Equation 5.3

The predictor $\hat{y}(x)$ takes the form of Equation 5.4 where β_0, β_i, β_{ii}, β_{ij} are unknown coefficients. Let β be a column vector containing the unknown coefficients.

$$\hat{y}(x) = \beta_0 + \sum_{i=1}^{m} \beta_i x_i + \sum_{i=1}^{m} \beta_{ii} {x_i}^2 + \sum_{i=1}^{m} \sum_{j \geq i}^{m} \beta_{ij} x_i x_j, \tag{5.4}$$

Equation 5.4

Theses coefficients can be solved for using Equation 5.5 and the least squares estimator, Equation 5.6. The minimum number of sample points p, is $p = (m+1)(m+2)/2$.

$$\beta = (U^T U)^{-1} U^T y_s, \tag{5.5}$$

Equation 5.5

$$U = \begin{bmatrix} 1 & x_1^{(1)} & \cdots & x_m^{(1)} & x_1^{(1)}x_2^{(1)} & \cdots & x_{m-1}^{(1)}x_m^{(1)} & \left(x_1^{(1)}\right)^2 & \cdots & \left(x_m^{(1)}\right)^2 \\ \vdots & \vdots & \ddots & \vdots & \vdots & \ddots & \vdots & \vdots & \ddots & \vdots \\ 1 & x_1^{(n)} & \cdots & x_m^{(n)} & x_1^{(n)}x_2^{(n)} & \cdots & x_{m-1}^{(n)}x_m^{(n)} & \left(x_1^{(n)}\right)^2 & \cdots & \left(x_m^{(n)}\right)^2 \end{bmatrix} \quad (5.6)$$

Equation 5.6

The Halton sequence is the chosen method for low discrepancy sampling [39]. It is a deterministic quasi-random number sequence that works by generalizing the van der Corput sequences [40]. The absolute minimum number of sample points for the case of two variables is six. To better map the response, 15 samples was used. The mean error was calculated from the resulting response surface to ensure that this number of sample points adequately covers the sample space. For the given ranges, Figure 5.4 shows the 15 points generated using the Halton sequence.

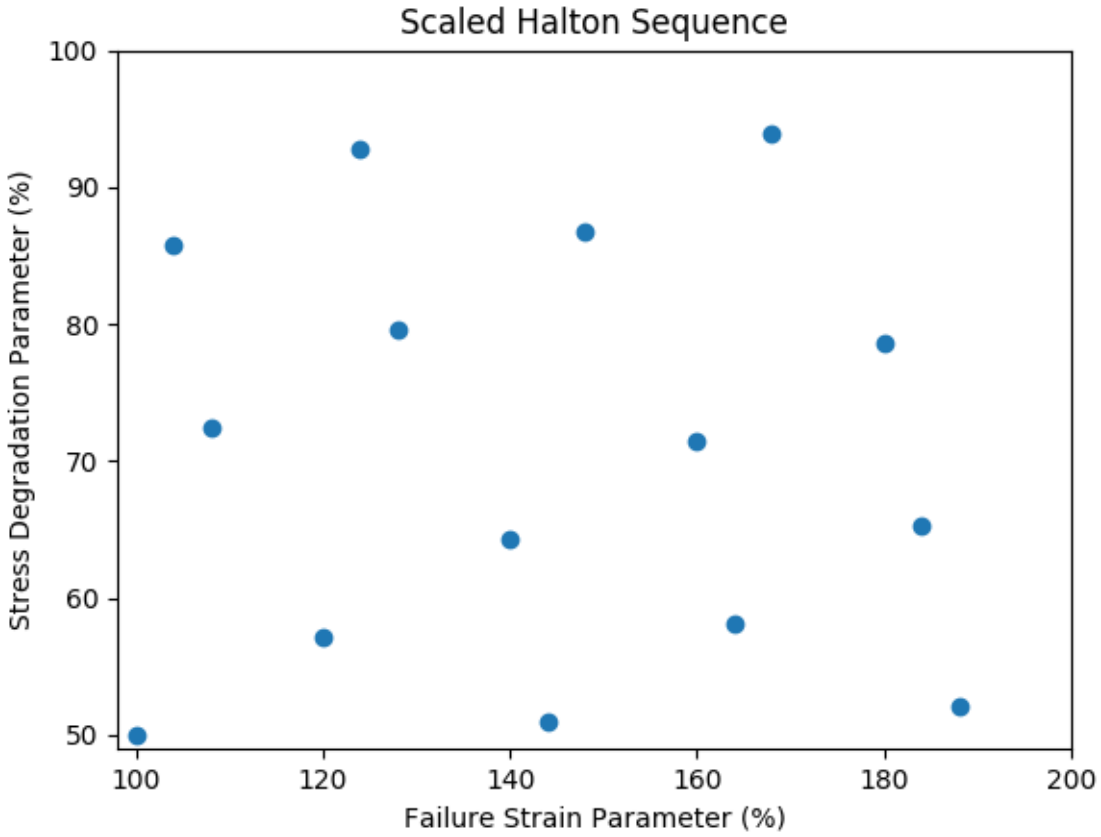

Figure 5.4. Scaled Halton sequence for the surface response method

5.3 Response Surface Results

The fifteen data points were run using the notched and unnotched geometries for each failure criteria. The response surface for each failure criteria is discussed in the following subsections.

5.3.1 Response Surface: Tsai-Wu

The results of the fifteen sampled points for the notched geometry are plotted below in Figure 5.5 and the corresponding response surface is shown in Figure 5.6.

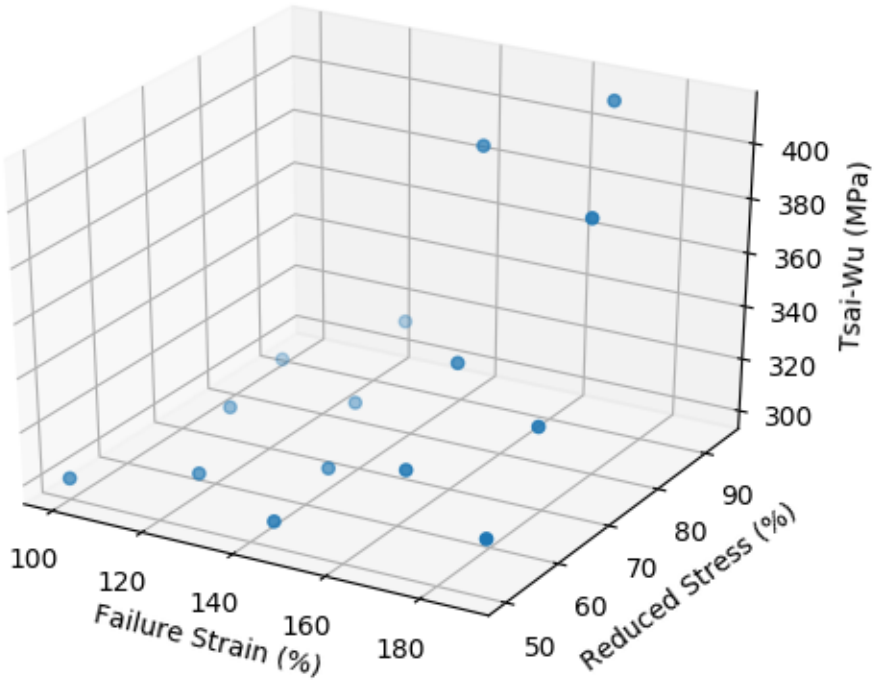

Figure 5.5. Stress results for the sampled data points (Tsai-Wu)

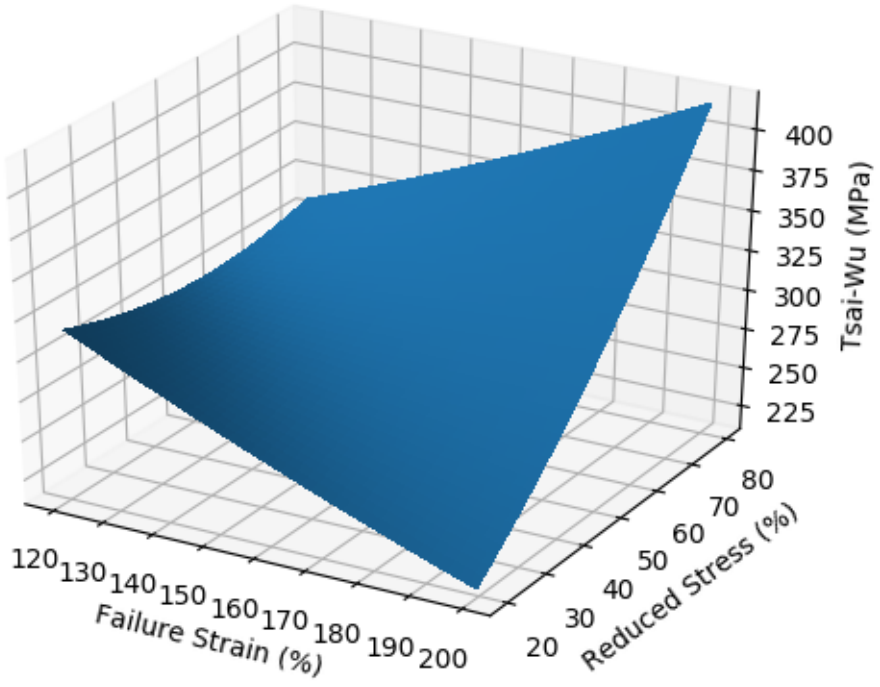

Figure 5.6. Response surface from the sampled points (Tsai-Wu)

The mean error between the sampled points, Figure 5.5, and the response surface, Figure 5.6, was found to be -0.45 MPa. The mean error value is low relative to the range of failure stress values, which indicates that the response surface is a good representation of the model for the range of sample points used. Figure 5.6 extends the range of the reduced stress parameter from 50% to 20% causing the failure stress to dip below the value of 301 MPa, the failure of the notched specimen using the Tsai-Wu failure criterion without the post-damage model. The response surface region around 301 MPa is not correct because the analysis will not fail before the failure criteria has initiated damage. The adjacent corner of low reduced stress and low failure strain can be seen trending upward. This is due to the lack of sample points in this range and could be amended in future work by using more sample points and possibly a cubic response surface. The general trend of the section of the plot that is affected by the post-damage model is that the reduced stress parameter has a greater effect on failure stress as the failure strain parameter increases. Similarly, the failure strain parameter has a greater effect on the failure stress as the reduced stress parameter increases.

For the instances in which the life of the specimen was effectively extended by the post-damage model, it did so by allowing the elements above and below the notch in the 0° and 90°

plies to retain some strength after failure. An example of the post-damage model having an effect is show in Figure 5.7.

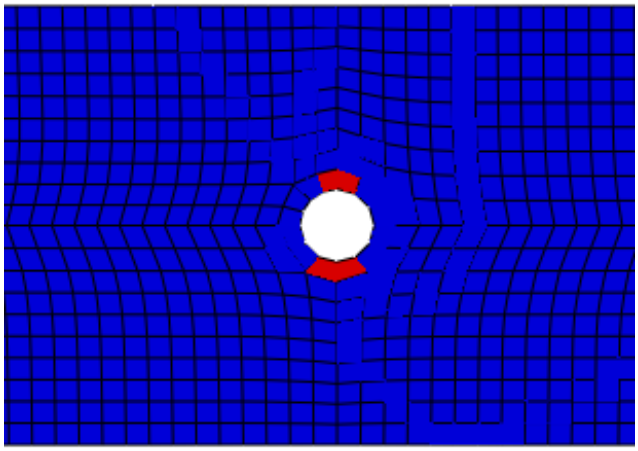

Figure 5.7. Failed elements which retained strength in post-damage

The failure strain and reduced stress parameters both contributed to increasing the specimen's life. A higher reduced stress factor would decrease the amount of strain the element would experience and an increased strain factor would allow an element with a lower stress to avoid deletion. Cases that resulted in the failure stress value that matched the analysis without a post-damage model dealt with elements that reached their strain limits too quickly. A test case was created in which no strain limit was placed on the element. Because no elements were being deleted, the laminate survived however, the strain far exceeded that which could bear the load.

The unnotched geometry was tested using the same sample points but was found to fail at the nominal failure stress for every sample point. Upon further investigation, it was found that elements became unstable after damage was initiated because of the stress level of the element being altered. This instability occurred in the unnotched laminate but not in the notched laminate because of the uniformity in the unnotched geometry. The notch in the notched geometry funneled stress to the notch making a clear stress gradient. The instability in the unnotched model is a result of many of the elements being at the same stress level and failing at approximately the same time. In an attempt to increase stability, several options were tested. Hourglass control was added through Abaqus' element selection. This decreased the deformations of the damaged elements but ultimately they were still unstable and failed after damage initiation. The post-damage model was changed from Figure 5.1 (c) to Figure 5.1 (a) in

hopes that avoiding a discontinuity in stress would stop the elements from becoming unstable. The change to Figure 5.1 (a) was ineffective at stopping the instabilities. Lastly, the analysis was tested using variants of the post-damage model in Figure 5.1 (a): one that kept stress constant after damage and another that used a positive slope to slowly increase stress after damage. Neither of these attempts were successful in curbing the instabilities and the post-damage model was considered to have no effect on the unnotched geometry.

The post-damage model was able to increase the life of the notched laminate but because of stability issues, it did not affect the life of the unnotched laminate. Because the model with the Tsai-Wu failure criteria over predicted the strength of the notched case and under predicted the strength of the unnotched case, the addition of the post-damage model is not particularly helpful in moving the failure stresses of either case closer to that of the physical specimen.

5.3.2 Response Surface: Maximum Stress and Hashin

The sampled data points were analyzed using the Maximum Stress and Hashin models for the notched and unnotched geometries. The parameters that enabled these models to sustain loads past damage initiation were far beyond the range of values used in the response surface. For example, the Maximum Stress failure criteria did not experience a change in failure load unless the reduced stress parameter was greater than 80% and the failure strain parameter was greater than 210%. These parameter values are not physically reasonable and so were not used.

The unnotched cases, similar to the Tsai-Wu results, also failed immediately for all parameters. The reason that the post-damage model affected the failure stress of the Tsai-Wu case and not the failure stress of the Maximum Stress and Hashin models is because Tsai-Wu is a fully interactive damage criterion.

At the notch, the point of greatest stress, stresses from each direction are present when the element fails. The Maximum Stress and Hashin cases do not consider both stresses in the fiber direction to contribute to failure simultaneously. This means that when the element does fail, the Maximum Stress and Hashin failure criteria only affects the post-damage model in one of the two fiber directions. Because the Tsai-Wu failure criteria is fully interactive, the post-damage

model has a greater effect allowing it to sustain loads when the Maximum Stress and Hashin failure criteria cannot.

5.3.3 Response Surface: Summary

A summary of the results of this chapter are presented in Table 5.1. While the post-damage model did not benefit the Tsai-Wu case directly, it is possible that it could be helpful once the model is further refined. The Tsai-Wu case will be used to test two more laminates against experimental data in Chapter 6 because it was able to closely predict the notched failure stress.

Table 5.1. Summary of the failure stresses for the failure criteria and post-damage models

	Notched Failure Stress (MPa)		Unnotched Failure Stress (MPa)	
	Failure Criteria	Post-Damage	Failure Criteria	Post-Damage
Physical Specimen	**295**	**295**	**578**	**578**
Tsai-Wu	301	301 to ~400	456	456
Maximum Stress	330	330	529	529
Hashin	327	327	529	529

6 VALIDATION & DISCUSSION

This chapter compares the Tsai-Wu failure model with two additional AS4 plain-weave laminates. No post-damage model will be used as it was not beneficial in the previous analysis. The results of these final analyses and the work as a whole will be discussed.

6.1 Laminate analysis

In addition to the first laminate layup, the two remaining laminates to be analyzed are shown in Table 6.1. The first laminate from the previous analyses is designated as 'A'.

Table 6.1. Remaining Laminates

Laminate	Layup
A	$[45/0/-45/90]2s$
B	$[45/-45/0/45/-45/45/-45/90/45/-45]s$
C	$[0/90/0/45/90/0/90/-45/90/0/90/45/0/90/0]$

The materials and geometries are the same as the first laminate but having additional layups will provide a better idea of how the damage model performs. The new laminates were run using the same FEM model and the Tsai-Wu failure criteria with no post-damage model. The results are summarized in Table 6.2.

Table 6.2. Summary of Tsai-Wu results using two new layups

	Notched Failure Stress (MPa)		Unnotched Failure Stress (MPa)	
Laminate	Tsai-Wu	*Physical Specimen*	Tsai-Wu	*Physical Specimen*
A	301	**295**	456	**578**
B	184	**298**	244	**373**
C	385	**347**	641	**675**

From the results in Table 6.2 it is clear that the model does not represent the physical specimen well. Looking at the layups tested, layup 'A' can be considered quasi-isotropic. Laminate 'B' has a greater number of 45° and -45° plies and laminate 'C' has a greater number of 90° and 0° plies. These laminate classifications can be used to draw conclusions from the results in Table 6.2. The

model provides the lowest stress predictions for laminate ‘C’ and the highest stress predictions for laminate ‘B’ relative to the physical specimen. The stress results from each classification of laminate points to the issue being with the model’s shear modulus. The shear modulus curve was extracted directly from the data sheet but it may be that some modification such as a change in slope is needed to better represent the physical results. Another issue seems to be the stresses at the notch. Laminate ‘C’ over predicted the stress in the notched laminate but under predicted the stresses for the unnotched laminate. Even without the shear modulus being an issue, the material model including the post-damage model would not provide good results for the notched case.

6.2 Discussion of Results

The research goals were stated in Chapter 1. The primary goals was to investigate the capabilities of a model using finite elements, failure criteria, and post-damage behavior to capture the failure of woven composite laminates under tensile loading conditions. The objectives that needed to be met to achieve these goals were as follows:

1. Implement a material model in Abaqus, a finite element solver, as a user-defined subroutine. The material model will use orthotropic and plane-stress assumptions to calculate stress.
2. Select a failure criteria that best represents plain-weave composite materials
3. Develop a post damage model that predicts the material’s behavior after damage occurs
4. Validate the model for notched and unnotched geometries using material data from NIAR

A macro-scale approach was chosen which consisted of a two-part damage model: damage initiation and post-damage. Damage initiation was controlled by a failure criteria and the post-damage portion degraded stresses to a constant level. Among the selected failure criteria, the Maximum Stress and Hashin theories provided the best results for the unnotched case and the Tsai-Wu results were closest for the notched case. The post-damage model used two parameters: a failure strain parameter that set a new limit for strain and a reduced stress parameter that gave the material a non-zero strength after damage had occurred. A range of different parameter values were used to evaluate the extent of the parameters’ effect. The only case that was affected

by the post-damage model was the Tsai-Wu failure criteria with a notched geometry for which its effect was not beneficial in better predicting failure stress. Lastly, the Tsai-Wu model without the post-damage portion was tested against two new layups. The results indicated that the shear modulus and stresses around the notch might not be correct. Although no additional testing was performed, it is believed that adjusting the shear modulus may help to improve the model.

The conclusions that can be drawn from this work fall into the categories of either failure criteria or post-damage model. Regarding failure criteria, for woven composite laminates, the Tsai-Wu failure criterion caused the model to fail at lower loads compared to the Maximum Stress and Hashin failure criteria. This was because the Tsai-Wu failure criterion considered the contributions of stresses in the non-loading direction more so than the Maximum Stress and Hashin failure criteria. The Tsai-Wu failure criteria closely approximated the failure stress for the notched geometry but severely under predicted the failure stress for the unnotched geometry. The Maximum Stress and Hashin failure criteria over predicted the failure stress for the notched geometry and under predicted the failure stress for the unnotched geometry but to a lesser degree than the Tsai-Wu failure criterion. Each failure criteria was conservative for the unnotched case, which is preferred when it comes to designing composites. None of the tested failure criteria were good approximations of both the notched and unnotched cases. The discrepancy between the failure criteria results and physical specimen is believed to be caused by the shear modulus. This was shown in Chapter 4 with further evidence seen in Chapter 6 section 6.1.

While the model whose results were closest to that of the physical specimen did not utilize a post-damage model, several insights were gained in the process. The post-damage model used, Figure 5.1 (c), was simple to implement and easy to manipulate. As seen in Chapter 5, the only failure criterion that was affected by the post-damage model was the Tsai-Wu failure criterion for the notched geometry. The unnotched geometries experienced instability that was unable to be resolved with hourglass control or different post-damage models. Due to not being fully interactive, the notched geometries for the Maximum Stress and Hashin failure criteria were unaffected by the post-damage model unless physically implausible values were used for the post damage-model parameters.

The Tsai-Wu failure criterion for the notched case saw effects from the post-damage model. The range of values chosen for the two parameters, reduced stress and failure strain, was 50% to 100% and 100% to 200% respectively. These values reflected what was thought to be physically possible for the material being used as well as values that were tested and shown to have an effect on the life of the specimen. A Halton sequence using fifteen points paired with a second-order response surface proved to be a strong representation of the chosen ranges, having a mean error of -0.45 MPa. The thresholds at which the specimen's life was extended was approximately 50% for reduced stress and 120% for strain. Values lower than this caused the model to fail at the same load as without the post-damage model. Because the response surface is a continuous surface, multiple combinations will cause the specimen to fail at the same load. The choice as to which combination for a particular failure load is best will come down to whatever best represents the physical phenomenon. With woven fabrics, the material is often quite brittle. To best represent a brittle material would mean using combinations that have lower values for the failure strain parameter and higher values for the reduced stress parameter. While the post-damage model was not used for the final model in this work, it seems that it would be useful for other models if the instabilities can be worked out.

Given the number of parameters in a problem such as modeling failure, many different paths could be taken to achieve better results. Based on the findings of this work, investigating different ways in which the shear modulus can be incorporated into the failure criteria is the next step to improving the material model. Something as simple as a coefficient could be applied to the shear modulus before performing the analysis. For a more mechanics-based approach, the model could incorporate meso-scale methods such as treating the shear modulus as a function of position given the sizes of the warp and weft fibers.

The approach taken in this work allows for computationally inexpensive analyses. As a macro-scale damage model, it simplifies much of the mechanics involved. While a model using a macro-scale approach can produce simulations that are practical and efficient, there are damage mechanics which are grossly oversimplified. The candidate models need to be validated before being implemented in industrial applications. Physical testing of multiple woven composite specimens was initially planned to take place at NASA Langley. This data would have [been

used to validate the results of this thesis. Unfortunately, due to scheduling issues, the testing date was pushed outside of the timeframe of this thesis making validation infeasible.

REFERENCES

[1] T. Johnson, "Composites In Aerospace," 2 April 2017. [Online]. Available: https://www.thoughtco.com/composites-in-aerospace-820418.

[2] N. Naik, Woven Fabric Composites, Philadelphia: Taylor and Francis, 1999.

[3] J. Fikes, "Composite Technology for Exploration," NASA, Huntsville, 2017.

[4] N. I. f. A. Research, "Hexcel 8552S AS4 Plain Weavev Fabric, Prepreg 193 gsm & 38% RC, Qualification Material Property Data Report," Wichita State University, Wichita, 2011.

[5] F. J and Y. Q, "Multiscale damage modelling for composite materials: theory and computational framework," *International Journal of Numerical Methods* , no. 52, pp. 161-191, 2001.

[6] M. H. Kashani and A. S. Milani, "Damage Prediction in Woven and Non-woven Fabric Composites, Non-woven Fabrics," in *Non-Woven Fabrics*, InTech, 2016, p. Ch. 10.

[7] I. M. Daniel, J.-M. Cho, B. T. Werner and J. S. Fenner, "MECHANICAL BEHAVIOUR AND FAILURE CRITERIA OF COMPOSITE MATERIALS UNDER STATIC AND DYNAMIC LOADING," *Meccanica,* 2014.

[8] M. J. Hinton, A. S. Kaddour and P. D. Soden, "A comparison of the predictive capabilities of current failure theories for composite laminates, judged against experimental evidence," *Composites Science and Technology,* vol. 62, no. 12-13, pp. 1725-1797, 2002.

[9] C. Sun, B. Quinn, J. Tao and D. Oplinger, "COMPARATIVE EVALUATION OF FAILURE ANALYSIS METHODS FOR COMPOSITE LAMINATES," U.S. Department of Transportation , Washington, D.C. , 1996.

[10] S. Tsai, THEORY OF COMPOSITES DESIGN, Dayton: Think Composites, 1992.

[11] S. G. O. L. L. T. P. Zinoviev, "Strength of multilayered composites under plane stress state," *Compos. Sci. Tech,* no. 58, pp. 1209-1224, 1998.

[12] L. J. Hart-Smith, "PREDICTIONS OF THE ORIGINAL AND TRUNCATED MAXIMUM-STRAIN FAILURE MODELS FOR CERTAIN FIBROUS COMPOSITE LAMINATES," *Composites Science and Technology,* no. 58, pp. 1151-1178, 1998.

[13] J. Z. Wang and D. F. Socie, "Biaxial Testing and Failure Mechanisms in Tubular G-10 Composite Laminates," *Composite Materials: Testing and Design,* vol. 11, no. ASTM STP 1206, pp. 136-149, 1992.

[14] L. Zhao, T. Qin, J. Zhang and R. A. Shenoi, "Modified maximum stress failure criterion for composite pi joints," *Journal of Composite Materials,* no. doi:10.1177/0021998312460713., 2012.

[15] S. W. Tsai and E. M. Wu, " A general theory of strength for anisotropic materials," *Composite Materials,* vol. 5, p. 58–80, 1971.

[16] H.-S. AHN, J.-H. KWEON and J.-H. CHOI, "Failure of Unidirectional-woven Composite Laminated Pin-loaded Joints," *Journal of REINFORCED PLASTICS AND COMPOSITES,* vol. 24, no. 7, pp. 735-752, 2005.

[17] University of Cambridge, "Failure of laminates and the Tsai–Hill criterion," [Online]. Available: https://www.doitpoms.ac.uk/tlplib/fibre_composites/laminate_failure.php. [Accessed 10 April 2018].

[18] R. Zahari, A. H. Azmee, F. Mustapha, M. S. Salit, R. Varatharajoo and A. Shakrine, "PREDICTION OF PROGRESSIVE FAILURE IN WOVEN GLASS/EPOXY COMPOSITE LAMINATED PANELS," *Jurnal Mekanikal,* no. 25, pp. 80 - 91, 2008.

[19] Z. Hashin, "Failure Criteria for Unidirectional Fiber Composites," *Journal of Applied Mechanics ,* vol. 47, pp. 329-334, 1980.

[20] A.Puck and H.Schürmann, "Failure analysis of FRP laminates by means of physically based phenomenological models," *Composites Science and Technology,* vol. 62, no. 12-13, pp. 1633-1662, 2002.

[21] K. C.Warren, R. A.Lopez-Anido, S. S.Vel and H. H. Bayraktar, "Progressive failure analysis of three-dimensional woven carbon composites in single-bolt, double-shear bearing," *Composites Part B: Engineering,* vol. 84, pp. 266-276, 2016.

[22] Z.-N. Feng, H. G. Allen and S. S. Moy, "Theoretical and experimental investigation of progressive failure of woven composite panels," *Journal of Composite Materials,* vol. 33, no. 11, pp. 1030-1047, 1999.

[23] A. Puck and H. Schurmann, "FAILURE ANALYSIS OF FRP LAMINATES BY MEANS OF PHYSICALLY BASED PHENOMENOLOGICAL MODELS," *Composites Science and Technology,* no. 58, pp. 1045-1067, 1998.

[24] J.-M. Bertholet and t. b. J. M. Cole, Composite materials: mechanical behavior and structural analysis, New York: Springer, 1999.

[25] G. Chu and C. Sun, "Failure Initiaion and Ultimate Strength of Composite Laminates Containing a Center Hole," *Composite Materials: Fatigue and Fracture,* vol. Fourth, no. 1156, pp. 35-54, 1993.

[26] P. P and R. C, "Progressive failure analysis of laminated composite plates by finite element method," *Journal of Reinfoced Plastics and Composites,* no. 21, pp. 1505-1513, 2002.

[27] T. Tay, G. Liu, V. B. C. Tan, X. S. Sun and D. C. Pham, "Progressive Failure Analysis of Composites," *Journal of Composite Materials,* vol. 42, no. 18, pp. 1921-1966, 2008.

[28] C. O, M. D, C. D, C. P and N. H, "Numerical modeling of nonlinearity, plasticity and damage in CFRP-woven composites for crash simulations.," *Composite Structures,* no. 115, pp. 75-88, 2014.

[29] T. Okabe, S. Onodera, Y. Kumagai and Y. Nagumo, "Continuum damage mechanics modeling of composite laminates including transverse cracks," *International Journal of Damage Mechanics*, 2017.

[30] P. Gudmundson and W. Zang, "An analytic model for the thermoelastic properties of composite laminates containing transverse matrix cracks," *International Journal of Solids and Structures,* no. 30, pp. 3211-3231, 1993.

[31] S. Murakami, Continuum Damage Mechanics – A Continuum Mechanics Approach to the Analysis of Damage and Fracture,, Dordrecht, Heidelberg, London, New York: Springer, 2012.

[32] A. Satyanarayana, P. Bogert, Kazbek.Z.Karayev, Paul.S.Nordman and H. Razi, "Influence of Finite Element Size in Residual Strength Prediction of Composite Structures," in *Structural Dynamics and Materials Conference*, Honolulu, 2012.

[33] M. Smith, "ABAQUS/Standard User's Manual, Version 6.9," Simulia, Providence, 2009.

[34] G. W. Milton, The Theory of Composites, Cambridge: Cambridge University Press, 2002.

[35] M. Hyer, Stress Analysis of Fiber-Reinforced Composite Materials, New York: The McGraw Hill Companies, 1997.

[36] W. E. Tsai SW, "A general theory of strength for anisotropic materials," *Composite Materials,* vol. 5, no. 1, pp. 58-80, 1971.

[37] Y. Murray and L. Schwer, "Implementation and Verification of Fiber-Composite Damage Models, Failure Criteria and Analysis in Dynamic Response," *ASME,* vol. 107, pp. 21-30, 1990.

[38] Z.-H. Han and K.-S. Zhang, "Surrogate-Based Optimization, Real-World Applications of Genetic Algorithms," in *Surrogate-Based Optimization*, Dr. Olympia Roeva, InTech, 2012, p. Chapter 17.

[39] J. Halton, "Algorithm 247: Radical-inverse quasi-random point sequence," ACM, 1964, p. 701.

[40] J. van der Corput, "Verteilungsfunktionen (Erste Mitteilung)," *Proceedings of the Koninklijke Akademie van Wetenschappen te Amsterdam*, vol. 38, p. 813–821, 1935.